Accepted Manuscript

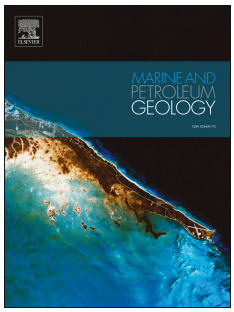

Depositional Model for a Prograding Oolitic Wedge, Upper Jurassic, Iberian basin

Luis Pomar, Marcos Aurell, Beatriz Bádenas, Michele Morsilli, Saad Fahd Al- Awwad

PII: S0264-8172(15)30004-0

DOI: 10.1016/j.marpetgeo.2015.05.025

Reference: JMPG 2254

To appear in: *Marine and Petroleum Geology*

Received Date: 3 March 2015

Accepted Date: 26 May 2015

Please cite this article as: Pomar, L., Aurell, M., Bádenas, B., Morsilli, M., Al- Awwad, S.F., Depositional Model for a Prograding Oolitic Wedge, Upper Jurassic, Iberian basin, *Marine and Petroleum Geology* (2015), doi: 10.1016/j.marpetgeo.2015.05.025.

Depositional Model for a Prograding Oolitic Wedge, Upper Jurassic, Iberian basin

Luis Pomar (a)*, Marcos Aurell (b), Beatriz Bádenas (b), Michele Morsilli (c) and Saad Fahd Al- Awwad (d)

a Departament de Ciencies de la Terra, University of the Balearic Islands, Palma de Mallorca, Spain

b Departamento de Ciencias de la Tierra, University of Zaragoza, Zaragoza, Spain

c Dipartimento di Fisica e Scienze della Terra, Università di Ferrara, Ferrara, Italy

d Geological Technical Services Department, Saudi Aramco, Dhahran, Saudi Arabia

* Corresponding author: luis.pomar@uib.es

Key words: infralittoral prograding wedge, oolitic shoal, carbonate ramp, Jurassic, bank-margin, clinobed

ABSTRACT

Facies architecture and bedding patterns of the Kimmeridgian Pozuel Formation (Iberian Basin) evidence that this 50-70-m thick oolitic-grainstone unit conforms to the Infralittoral Prograding Wedge (ILPW) model instead of the classic models used for interpreting oolitic grainstones sandbodies on carbonate ramps or platforms (i.e., bank-margin shoal complexes, beaches and beach ridges).

Ten lithofacies have been distinguished in the Pozuel Formation: 5–10° dipping clinobedded oolitic gra instone foresets passing to tabular oolitic packstones-grainstones, which interfinger the muddy basinal bottomsets. Landwards, the clinobeds pass into subhorizontal topsets composed of trough cross-bedded to structureless oolitic grainstones; oolitic-skeletal grainstones with stromatoporoids and coral-stromatoporoid-microbial mounds. Siliciclastic lithofacies and oncolitic/peloidal packstones occur at the innermost position. These lithofacies stack in strike elongated, 5–20-m thick, 0,5-2 km dip-oriented wide, aggradational-progradational packages with complex sigmoid-oblique geometries.

Lithofacies, depositional geometries and stacking pattern permit to summarize the main characteristic of such Upper Jurassic oolitic infralittoral prograding wedge potentially to be applied in other oolitic sandbodies both in outcrops and subsurface: 1) sediment production within the wave action zone, 2) grainstone-dominated textures, 3) prograding basinward onto basinal muds, 4) laterally (strike) extensive, paralleling the shoreline, 5) variable thickness, commonly of few tens of meters, 6) broadly sigmoidal to oblique internal architecture, with topsets, foresets and bottomsets, 7) dip of foresets close to the angle of repose, 8) topsets deposited in shallow-water, extending through the shoreface, from the shoreline down to the wave base, 9) mounds, either microbial or skeletal, may occur in the topsets.

The coated-grains factory was along the high-energy, wave-dominated outer platform (topset beds), from where the mud was winnowed and the grains transported both landward to the platform interior, and seaward to the platform edge, from were the grains cascaded down the slopes as grain flows and mass flows, forming clinobeds. This genetic model can be applied to other grain-dominated lithosomes, some of them forming hydrocarbon reservoirs, e.g., the Jurassic Hanifa Formation and some Arab-D (e.g., Qatif Field) in Arabia, the Smackover Formation in northern Louisiana and south Arkansas, the Aptian Shuaiba Formation (e.g., Bu Hasa Field) and the Cenomanian Mishrif Formation (e.g., Umm Adalkh Field) of the Arabian Gulf.

1. Introduction

Depositional models are the figurative expression of the concepts we use to explain the processes operating in the formation of sedimentary rocks. This is the reason why in stratigraphic reservoirs, exploration targets and production strategies are constrained by the prevailing depositional and stratigraphic models. And this also signifies that recognition of new stratigraphic details can induce a redesign of the production strategies through promoting more realistic models for characterization of the inter-well heterogeneities. Similarly, enhanced visualization of stratigraphic details can improve the understanding of

carbonate lithosomes and may trigger new exploration opportunities and renewed exploration interest even in mature reservoirs.

Studies of modern sedimentary environments are fundamental in building depositional models because they provide the characteristics of sediment accumulations in relation to processes, though predictive models for inter-well-scale variations in heterogeneous rocks are best made from outcrop studies. In carbonate rocks the study of outcrop analogs has an additional interest due to the dependence of sediment production to evolving biology and the reliance of carbonate production on environmental conditions. Besides the specific paleogeographic and geotectonic context, carbonate platform successions have distinctive characteristics that reflect the physical, chemical, and biological conditions to that specific Phanerozoic window (Read, 1998; Pomar, 2001a; Mutti and Hallock, 2003; Bosence, 2005; Pomar and Hallock, 2008; Pomar and Kendall, 2008; Westphal et al., 2010).

Thus, construction of precise depositional models from outcrop studies is contingent for subsurface carbonate reservoirs. Those provide static descriptive models for comparison to contemporaneous reservoir heterogeneity styles. Nevertheless, the analysis of the processes involved in the stacking of facies and in the creation of the heterogeneities, adds an extra value to the model, particularly in carbonates. Based on processes analogies, genetic analysis can induce models to become time independent, except for the time-specific carbonate-producing biota, and can thus become more valuable for interpretation and prediction.

The Upper Jurassic Pozuel Formation, exposed along a 15-km-long, northeast-southwest transect, in the Sierra de Albarracín, west of Teruel (Iberian Range, eastern Spain), is an oolitic carbonate platform that prograded with low-angle (5º to 10º) clinoforms. These outcrops provide an excellent opportunity to build a genetic model that can be applied to other prograding grain-dominated lithosomes, usually interpreted as oolitic shoals, some of them forming hydrocarbon reservoirs, e.g., the Jurassic Hanifa Formation and some Arab-D (e.g., Qatif Field) in Arabia, the Smackover Formation in northern Louisiana and south Arkansas, the Aptian Shuaiba Formation (e.g., Bu Hasa Field) and the Cenomanian Mishrif Formation (e.g., Umm Adalkh Field) of the Arabian Gulf.

Large-scale cross-bedded lithosomes deposited in shallow-water settings are common reservoirs in both lithoclastic and carbonate systems, and multiple models have been built to explain their characteristics and origin. In lithoclastic systems, the variability of models is derived from the diversity in location of both the sediment source and processes controlling

sand accumulation. In carbonate systems, diversity of existing models is also dependent on the diversity of the source of the grains, location of the source, changing ecological conditions that affect the carbonate-producing biotas, and in the redistribution processes. Most common models for marine carbonate cross-bedded lithosomes are the sand shoals and beaches, tidal bar belts, marine sand belts, platform interior sand blankets, flood- and ebb-tidal deltas, etc. (e.g., Ball, 1967; Halley et al., 1983, Harris, 2009). Bank-margin carbonate sands occur repeatedly throughout the geologic record and, although it is tempting to use the distribution of bank-margin sands in South Florida and the Bahamas for interpreting ancient deposits, they do not represent all accumulation types in the geologic record. Here we build a genetic depositional model for large-scale cross-bedded lithosomes deposited in wave-dominated shallow-water seas, based on the outcrop study of the Pozuel Formation in the Sierra de Albarracín (Spain) along with the comparative analysis of other examples from outcrops and subsurface.

2. Geological setting; the Kimmeridgian Pozuel Formation

Kimmeridgian (Upper Jurassic) limestones crop out between the villages of Frías de Albarracín and Moscardón (**Fig. 1A**) west of Teruel, Iberian Range. These rocks consist of oolitic and skeletal limestones with variable amount of sandstone and marls, which conform the 50- to 70-m-thick Pozuel Formation (Aurell et al., 1998; Bádenas and Aurell, 2001).

During the Kimmeridgian, shallow epeiric seas covered wide areas of Western Europe **(Fig. 1B)**. Terrigenous sedimentation occurred to the north, whereas to the south, carbonate sedimentation dominated the Iberian Basin, facing the Tethys Ocean to the west on the western margin of the Iberian Plate (e.g., Dercourt et al., 1993). On the Iberian Basin, wide carbonate ramps developed at around 20–25º N paleolatitude (Osete et al., 2011) with low-angle depositional slopes from shallow areas to relatively deep-water outer areas (e.g., Aurell et al., 2003). In the Kimmeridgian sedimentary succession, two third-order depositional sequences (Kim1 and Kim2) have been recognized in the central part of the Iberian Basin (Aurell et al., 2003; Bádenas and Aurell, 2010). The overall facies distribution shows the progradation of the shallow-ramp (Pozuel and Torrecilla formations) over the outer-ramp lime mudstones and marls of the Sot de Chera and Loriguilla formations (**Fig. 1C).**

The present study concentrates on the Pozuel Formation, the shallow facies belt in the upper part of the Kim1 sequence **(Fig. 1C).** In the underlying Sot de Chera Formation, ammonites of the *Planula* (uppermost Oxfordian) and *Platynota* (lowermost Kimmeridgian)

zones occur. On top of the Pozuel Formation, the discontinuity between the Kim1 and Kim2 sequences was developed at the onset of the upper Kimmeridgian (i.e., *Acanthicum* Zone: Bádenas and Aurell, 2001).

Our approach is based on facies mapping on photomosaics and on stratigraphical log descriptions of three localities: around Frías de Albarracín and Moscardón villages and in a roadcut between Frías de Albarracín and Calomarde **(Fig. 1A).** The study has been complemented with the analysis of 65 thin sections and polished slabs, to characterize components and textures. Mapping of facies architecture was made onto panoramic photographs taken from hills and with a small drone flying at low altitude. Critical surfaces and lithofacies were mapped in the field by walking on the outcrop faces. Depositional dip angles were measured when possible.

3. Facies description

The Pozuel Formation in the Sierra de Albarracín consists of a dominantly oolitic limestone, with minor contribution of other calcareous components and some terrigenous. It is sandwiched between the siliciclastic dominated Sot de Chera Formation below and the sandstones and marls of the Torrecilla Formation on top. Within the Pozuel Formation lithofacies (LF1–LF10) have been distinguished on the basis of components and sedimentary structures and their relative position, from distal (LF1) to proximal settings (LF10) (**Table 1**).

3.1.- LF1- Marls and intercalated oolitic sandstones and wackestones

This lithofacies mainly consists of marls with abundant mica and plant remains, and scarce bioclasts (bivalves, brachiopods, gastropods and foraminifera). They include up to 30-cm-thick intercalations of fine-grained sandstones to silty limestones, locally with parallel and cross-lamination (LF2; **Fig. 2A**). Vertical and lateral transition to LF2 oolitic packstones-grainstones is reflected by the increase in ooids and carbonate matrix in both marly beds and sandstone-silty limestone beds (**Fig. 2B**). These oolitic marly wackestones have ubiquitous bioturbation, including *Planolites*, *Thalassinoides* and *Chondrites* traces, and commonly form meter-scale marl-limestone alternations. Ooids are fragmented and ferruginized, and variable in size (**Fig. 3A**). Cortices have thinly fine-radial laminae or alternating micritic and fine-radial laminae. Nuclei are mostly quartz grains, but also bioclasts and peloids.

LF2- Oolitic packstones-grainstones

Oolitic packstones-grainstones occur at the transition from the marly sediments (LF1) to the oolitic clinobeds (LF3) as 0.2–0.4 m-thick tabular beds interbedded with few-cm-thick marly beds (**Fig. 2A, B, E**). Bioturbation is less intense than in LF1 (**Fig. 2C**). Locally, medium-scale cross bedding occurs. Main components of this lithofacies are ooids, with variable size (1 mm on average). Cortices and nucleus are similar to those of ooids in LF1. Minor components are sand-sized quartz grains, peloids and bioclasts. Brachiopods, echinoids and scallops are frequent.

LF3- Clinobedded oolitic grainstones

Oolitic grainstones (LF3) with large-scale low-angle clinobeds is the most outstanding lithofacies. Dip angle of clinobeds ranges between 5º to 10º basinward. Thickness of individual beds usually ranges between 0.2 to 0.5 m, and thickness of clinobed sets varies between few meters (Frías; **Fig. 2D**) to more than 10 m (Moscardón; **Fig. 2E**). The oolitic grainstones include variable-sized ooids and are well to moderately sorted (**Fig. 3C to F**). In the moderately sorted oolitic grainstones, parallel lamination is visible within the beds, whereas the well-sorted beds are structureless (**Fig. 3C**). Small ooids have thinly laminated fine-radial cortices, whereas larger ooids have thin alternating fine-radial and micritic laminae. Nuclei are mainly quartz grains, and less frequent bioclasts and peloids (**Fig. 3E**). Minor components are oncoids (up to 0.5 cm in diameter) with thinly laminated micritic cortices, sand-sized quartz grains, peloids, and mm-sized bioclasts (bivalves, brachiopods, gastropods, foraminifera, echinoderms, bryozoans, corals, algae, and serpulids). Levels dominated by compound ooids, aggregated ooids and oolitic intraclasts are also present at the lowermost part of some clinobeds (**Fig. 3F**).

LF4- Trough and planar cross-bedded oolitic grainstones

This lithofacies occurs with two different cross-bed dimensions. Trough cross-bedded oolitic grainstones (LF4-1) occur in sets up to 50 cm thick (**Fig. 4A**). Isolated sets (up to 2 m thick) of large-scale planar cross-bedded grainstones (LF4-2) are visible in the middle-upper part of the Frías section (**Fig. 4B**). Grainstones are composed by variable-sized ooids, usually very-well- to well sorted (**Fig. 4C, D**). Ooids with alternating fine-radial and micritic laminae and quartz grains in the nuclei, dominate. Bioclasts similar to those of LF3, sand-sized quartz grains and mm-sized quarzite pebbles are also present.

LF5- Structureless to poorly laminated oolitic grainstones

This lithofacies consists of well-sorted oolitic grainstones arranged in 0.3- to 1-m-thick tabular beds, with poorly developed parallel to undulate lamination, or structureless, or with bioturbation (**Fig. 4E**). Ooids are similar to those of LF4, but in certain beds compound ooids dominate (**Fig. 4F**).

LF6- Oolitic-skeletal grainstones with stromatoporoids

Oolitic-skeletal grainstones with stromatoporoids (LF6) occur either as extensive but thin (≈ 30-cm thick) beds, or as dm-thick lenticular to channel-like beds, up to ten meters wide (**Fig. 5**). This lithofacies is characterized by the occurrence of large and abundant stromatoporoids (including chaetetids such as *Solenopora* and *Pychochaetetes*; Fezer, 1988) surrounded by skeletal-oolitic grainstone matrix (**Fig. 6A**). Stromatoporoids are in living position within the laterally extensive beds, but also in cm-sized fragments in the lower parts of the lenticular and channel-like beds. Other skeletal components are echinoderms, bivalves, gastropods, corals, foraminifera and algae. Ooids have thin alternating fine-radial and micritic laminae and bioclasts and quartz grains at their nuclei. Compound ooids, intraclasts of oolitic facies, and poorly rounded fragments of microbial crusts are also present (**Fig. 6 B**).

LF7- Mounds

Mounds can either be dominated by metazoans (**LF7-1**) or by microbial crusts (**LF7-2**), and they are about few decimeters thick and few meters wide (**Fig. 5**). Metazoans are usually in growth position and include corals (*Stylina tubulifera*, *Stylina parcicostata*, *Stylina* sp. *Comoseris minima*, *Comoseris meandrinoides*, *Heliocoenia variabilis*, *Microphyllia minima*) and stromatoporoids (including chaetetids) (Fezer, 1988). Metazoan-dominated mounds (**LF7-1**) result from the stacking of small stratiform beds (**Fig. 5**). Corals and stromatoporoids are surrounded by discontinuous microbial crusts with micro-peloidal microfabrics and micro-encrusters (mainly *Koskinobullina*, *Tubiphytes-Crescentiella*, bryozoans and serpulids; **Fig. 6C**). Internal cavities are filled by mud-supported sediment with variable proportions of fine-sand quartz grains, ooids, bioclasts (mainly echinoderms) and fragments of microbial crusts. Borers include bivalves and sponges. Microbial crust-dominated mounds (**LF7-2**) have also corals and stromatoporoids, usually in growth position, but microbial crusts with micro-peloidal microfabric and abundant *Tubiphytes-Crescentiella* predominate (**Fig. 6D**). In macroscopic view, crusts show bush-like dendrolite

fabric (**Fig. 5E**). Serpulids, bryozoans, and boring sponges are also present, and small internal cavities are filled by muddy sediment.

LF8- Intraclastic-oolitic packstones-grainstones with quartz

Lithofacies LF8 mostly occurs as inter-mound sediments (**Fig. 5**). Laterally equivalent and coeval to the metazoan-dominated mounds (LF7-1), LF8 consists of decimeter-thick fine-grained sandy intraclastic-oolitic beds with thin marly intercalations and sandy quartz. It is characterized by: some fine-sand quartz grains, poorly rounded intraclasts made of microbial crusts, bioclasts (echinoderms, metazoans, bivalves, gastropods and foraminifera) and variable proportion of ooids (**Fig. 6E, F**). This lithofacies is coarser and more cemented in beds coeval to microbial-crust dominated mounds (see level 4 in **Fig. 5**). Upwards in the succession, there is an increase in ooids and quartzite pebbles (see level 5 in **Fig. 5**).

LF9- Mudstones, sandstones and conglomerates

Lithofacies LF9 is well exposed in a gully, to the northwest of Frías (**Fig. 7**). It mainly consists of sandstones and conglomerates, with variable proportion of ooids and quarzite and carbonate pebbles. Different sandstone lithosomes occurs. High-angle planar cross-bedded sandstones (LF9-1) with eastern-dipping and 25º mean dip angle pass, downdip into trough cross-bedded sandstones (LF9-2) and these, in turn, pass vertically to eastern-dipping low-angle large-scale cross-bedded sandstones (LF9-3). Planar cross-bedded sandstones with low-angle, western-dipping cross-beds, and intercalated bioturbated mudstones (LF9-4) are on top of LF9-3. The succession ends with two conglomerate beds including mm- to cm-sized quarzite and carbonate pebbles. In the Calomarde roadcut, tabular dm-thick sandstones beds with intercalated cm- to dm-thick mudstones (LF9-6) are interbedded with carbonate lithofacies LF5, LF8 and LF10.

LF10- Oncolitic/peloidal packstones

This lithofacies is locally recognized in the uppermost part of the studied succession near Frías (**Fig. 5)** and in the Calomarde roadcut**.** It encompasses dm-thick tabular packstone beds, either dominated by oncoids or by peloids, with variable proportions of bioclasts (corals, stromatoporoids, gastropods, bivalves, foraminifera), intraclasts (microbial crusts and silty mudstones) and ooids. Oncoids size ranges from mm to few cm, and have thick cortices with thin micritic laminae and bioclastic or intraclastic nuclei. Peloids range from

lithic peloids (small micritic intraclasts) to micro-peloids. Peloid-dominated packstones are usually bioturbated.

4. Facies architecture

The oolitic Pozuel Formation conforms an overall shallowing-upward succession (e.g., Bádenas and Aurell, 2001) in which the vertical and lateral lithofacies distribution reflects the stacking of basic accretional sedimentary units. These accretional units are bounded by sharp surfaces marked by abrupt facies shifts and, locally, associated to erosion. They represent either basic sequences or parasequences. The downdip extension of the accretional units varies from 0.5 km to 2 km and their thickness ranges from 5 m to 20 m.

4.1.- Moscardón

Cliffy outcrops west of Moscardón offers the opportunity to study the 2D facies architecture of the Pozuel Formation in an almost dip transect, and at both large and small scale (**Fig. 8**). There, 9 accretional units, 10- to 20-m thick, can be analyzed (**Fig. 8B, C**). The most conspicuous lithofacies are the clinobedded oolitic grainstones (LF3) that form the cliffy outcrop (**Fig. 8A**). In units M2 to M7, the clinobedded grainstones pass downdip into oolitic packstones-grainstones (LF2) and into wackestones interbedded with marls (LF1). Clinobeds progradation in units M2, M3 and M8 is to 110º–130º (SE), with slope angles ranging from 7º to 12º. Updip, the clinobedded grainstones (LF3) pass into trough cross-bedded grainstones (LF4-1) that do not form clean exposures (see units M5 and M6).

Boundaries of accretional units are marked by abrupt facies shifts. Small metazoan-dominated mounds (LF7-1) occur on top of clinobedded grainstones of unit M6 (**Fig. 8A**). They occur associated to cross-bedded oolitic sandstones with local hummocky cross-stratification (LF9-2), and they are both overlaid by a second group of metazoan-dominated mounds, and all them pass downdip into bioclastic marls.

4.2.- Frías de Albarracín

Near Frías, the facies architecture of the Pozuel Formation can be seen on a cliffy outcrop that provides a clean and nearly undisturbed section in oblique direction (**Fig. 9**). Some incisions on the cliff provide small windows of the facies architecture in dip direction. Five accretional units, bounded by prominent bedding surfaces can be traced all across the studied outcrop. These accretional units can either be parasequences or basic depositional sequences. The lower unit F1 crops out in a limited area and consists of cross-bedded

sandstones and oolitic sandstones (LF9-2). This unit is sharply overlain by unit F2, with trough cross-bedded oolitic grainstones (LF4-1) in the lower part and evolving vertically into structureless to poorly laminated grainstones (LF5). Unit F3 mostly consists of structureless (LF5) overlaid by cross-bedded (LF4-1) oolitic grainstone, that is in turn overlain by clinobedded oolitic grainstones (LF3) and an upper interval of structureless LF5 and oolitic-skeletal LF6 grainstones on top. Interbedded in this upper interval there is a single bed with unidirectional planar cross-bedding (LF4-2). Clinobeds in unit F3 indicates an eastward progradation (070º–110º) with dip angle ranging from 6º to 12º. The planar cross-bedding (LF4-2) in the upper interval indicates unidirectional south-westward migration (140º–150º) with 20º foreset dip angle. Units F2 and F3 have similar thickness, around 15-20 m. After a prominent surface, a more recessive skeletal-dominated unit F4 occurs. It consists of a 5-m-thick (oolitic-skeletal grainstones with stromatoporoids (LF6) overlain by metazoan-dominated mounds and inter-mound sediments (LF7-1 and LF8). Unit F5, above an erosion surface, encompasses microbial crust-dominated mounds and inter-mound sediments (LF7-2 and LF8) that pass vertically into oncolitic/peloidal packstones (LF10).

4.3.- Calomarde roadcut

Along the road from Calomarde to Frías de Albarracín, a roadcut exposes almost the entire vertical succession of the Pozuel Formation. There, the overall shallowing-upward facies succession is punctuated by prominent bedding surfaces that bound the basic accretional units. These accretional units can either be parasequences or basic depositional sequences. Up to seven accretional units can be recognized in the lower part of the oolitic succession, below a prominent erosion surface (C1 to C7; **Fig. 10)**. Above this erosion surface, alternations of LF5, LF8, LF9 and LF10 occur, but bedding perturbation and faults impede a detailed identification of the accretional units.

In the lower part of the section, accretional unit C1 is a 2-m-thick alternation of oolitic packstone-grainstone and clay layers (LF2) deposited above the marly lithofacies (LF1). It is sharply overlain by the second accretional unit C2, composed by 5-m-thick clinobedded (LF3) and trough cross-bedded oolitic grainstones (LF4-1) and a thin marly bed on top. Subsequently, unit C3 consists of around 4-m-thick trough cross-bedded oolitic grainstones (LF4-1), overlain by structureless grainstones (LF5). Unit C4 is still composed by cross-bedded LF4-1 grainstones but the overlaying LF5 structureless grainstone lithofacies becomes thicker. Units C5, C6 and C7 consist of structureless grainstone lithofacies (LF5),

the uppermost of those containing small buildups, and overlain, in turn, by sandy intraclastic-oolitic packstones-grainstones (LF8) that marks the onset of siliciclastic input.

5. Depositional model

The analysis of bedding patterns, components and sediment textures of individual lithofacies and the recurrence in lithofacies successions (Walther's law) within the accretional units, permit elaboration of a depositional model (**Fig. 11**).

The ten lithofacies (LF1–LF10) described above belong to a continuous spectrum of sub-environments, from the shoreline to the shallow basin. Clinobedded oolitic grainstones (LF3) is the most outstanding lithofacies (foresets). Basinward, it toes out asymptotically on the muddy basinal deposits (bottomsets) with a downdip decrease in ooid content (LF2 and LF1) (**see Fig. 8)**. Landward, it changes into subhorizontally bedded (topsets) trough and planar cross-bedded oolitic grainstones (LF4) and these, in turn pass into structureless to poorly laminated oolitic grainstones (LF5) (**see Figs. 8 and 9**). Updip, the proportion of skeletal components increases, and oolitic-skeletal grainstones with stromatoporoids (LF6), mounds (LF7) and related inter-mound sediments (LF8) appear. At the innermost part of the topsets, siliciclastic lithofacies (LF9) and local oncolitic/peloidal packstones (LF10) occur (**see Fig. 7 and 9**).

The clinobedded lithosome (LF3) is interpreted to be the result of avalanche below the wave base, of sediments swept seaward from the friction-dominated zone during events of intense wave action (e.g. Swift et al., 1985; Nummedal, 1991). Although the angle of the clinobeds (5º-10º) and the sorting may induce to think on beachface deposits, or even on "sharp based shoreface sequences" (*sensu* Plint, 1988), the thickness and the spatial facies relationships exclude this interpretation and indicate these clinobeds to result from sediment accumulation from avalanching below the base of waves (**Fig. 11**). Sediments avalanched onto the slope might also be moved along slope by currents parallel to shoreline. Variable-sized ooids and oolitic limestone intraclasts in the clinobeds indicate different hydrodynamic-energy events on the platform top where they were generated, and from where they were shed off bank. Content of resedimented ooids progressively decrease from the clinobeds (LF3) to basinal areas (LF2 and LF1). Thus, these clinobeds do not represent the migration of large bedforms but a region of the coastal-equilibrium profile where sediments accumulate below the base of wave action. This slope migrates according to the sediment supply and the available accommodation, and perfectly fit in the “clinothem” deposits concept of Rich (1951).

The topset lithofacies deposited above the clinobedded lithosome. The trough and planar cross-bedded grainstones (LF4) were deposited at the outer part of the shelf, where the main oolitic factory was located. In this oolitic belt, the SSE migration of small 3D dunes (LF4-2) indicates an oblique transport respect to the paleo-margin (**Fig. 11**), which was mostly N-S oriented during deposition of unit F3 in Frías (**see Fig. 9**). In this setting, the ooids were transported alongshore by currents, but also shed off from the platform top, down the slope. This downdip sediment transport was responsible of the clinobeds progradation.

Landward of the trough cross-bedded oolitic facies belt (LF4-1), the structureless to poorly laminated oolitic grainstones (LF5) and oolitic-skeletal grainstones (LF6) represents a calmer area where burrowing became active on a more stable sandy seafloor. On these sand blankets, organic churning was so extensive that individual burrows became obscured. Locally, isolated subaqueous dunes (planar cross-bedded LF4-2) migrated. In this steady setting, metazoans (stromatoporoids), as well as other shelled organisms, first started to grow and contributed to increase the skeletal components (LF6). Farther landward, metazoans (corals and stromatoporoids) and microbes formed small mounds (LF7-1). Between the mounds, currents transported ooids updip and mixed them with bioclasts and intraclasts derived from the mounds (i.e., inter-mound LF8 sediments). Lenticular and channel-like beds recorded in LF6 (**see Fig. 5**) reflect up- and down currents that, although speculative, might have been induced by storms.

In the innermost part, microbial-dominated mounds (LF7-2) with abundant *Tubiphytes-Crescentiella* held corals and stromatoporoids (**Fig. 11**). Between the small mounds, siliciclastics brought from a nearby terrigenous littoral system where admixed with angular intraclasts derived from the mounds. The angularity of the intraclasts in these inter-mound sediments and the increasing content in quartzite pebbles to the top indicate minor transport and proximity of the terrigenous source area. This terrigenous littoral system is well exposed in the gully northwest of Frías (**see Fig. 7**). There, the oolitic limestone is overlain by a sandstone and conglomerate bed (LF9). This sandstone bed (Fig. 7 A and E) consists of small delta foreset (high-angle planar cross-bedded sandstones), and a series of shingling stacked shoreface (trough cross-bedded sandstones), foreshore (low-angle cross-bedded sandstones), and backshore-berm sub-environments (cross-bedded sandstones and intercalated bioturbated mudstones). The shingling stacking of these sandy lithosomes records deposition in a forced regression context and marks the end of carbonate

deposition in this area. Supralittoral deposition would also include small lagoons with favorable conditions for oncoid and peloidal sediment deposition (LF10).

5.1.- Outcrops correlation and architecture of sequences

Reconstructing the overall facies architecture of the oolitic body by the correlation of the three separated outcrops is challenging because of the absence of a continuous outcrop and by the clinobedded nature of the oolitic facies belts, which precludes a bed-by-bed "layer-cake" correlation. Although the correlation between Frías, Calomarde roadcut and Moscardón outcrops is highly uncertain, a speculative cross section in the direction of progradation can be built (**Fig. 12)** incorporating the dimension of the accretional units (5- to 20 m thick; 0.5- to 2 km downdip extension), the sigmoidal-oblique configuration and the actual stacking of the basic accretional units at each locality.

In Moscardón, a simple aggradational-progradational pattern of the accretional units is visible (**Fig. 8**). In Frías, the stack of accretional units is characterized by an overall aggradation-progradation trend with an internal pulse of retrogradation, recorded by the small wedge of clinobedded oolitic grainstones LF3 intercalated in unit F3 (**Fig. 9**). This stack of accretional units reflects the architecture of a TST and HST within a depositional sequence. In Calomarde roadcut (**Fig. 10**), thickness variations and facies shifts across boundaries also indicate an overall progradation, with a lower part (C1 to C4) characterized by a progressive increase in accommodation (TST), followed by a decrease (C5 to C7), that culminated with siliciclastic input at the top of unit C7 (HST). The inner lagoonal facies above the sharp erosion surface atop of unit C7 belongs to a subsequent depositional sequence.

Finally, the construction of this cross section requires assuming the occurrence of intervening downward shifting segments to compensate the aggradational ones. The resulting cross section made from Frías to Moscardón (**Fig. 12**), despite being highly speculative, illustrates a possible compartmentalization in dip direction, resulting from the shingling stack of three depositional sequences of about 50-m thick and 1- to 2-km wide sedimentary bodies.

6. Discussion; bank margin shoals, beaches and infralittoral prisms

The clinobedded oolitic lithosomes in the Pozuel Formation west of Teruel does not fit some of the prevailing models used for interpretation of ancient grain-supported large-scale cross-

bedded bodies: bank-margin shoal complexes, beaches and beach ridges. The oolitic clinobedded lithosomes prograded below the wave base downlapping and interfingering with basinal muds. The accretional style of the oolitic Pozuel Formation conforms with the "*infralittoral prograding wedge*" (ILPW) model (*sensu* Hernández-Molina et al., 2000), a progradational platform-margin slope, in which topset, foreset, and bottomset beds can be recognized.

6.1.- The bank-margin shoal complexes

Bank-margin carbonate sands occur repeatedly throughout the geologic record and are prominent elements of carbonate facies models. The distribution and composition of these banks in Southern Florida and the Bahamas are very well known (Rankey et al., 2006; Rankey and Reeder, 2011; Sparks and Rankey, 2013; Purkis et al., 2014) and often it is tempting to interpreted ancient deposits to fit these modern examples, even when differences are notable. Requirements for bank-margin carbonate sands to form are the existence of sand-sized sediments and a means for sorting them. These conditions are met where a change in shelf slope coincides with wave action or strong tidal currents in a zone of high carbonate production (Harris, 2009). Despite modern ooid shoals have been extensively studied, Sparks and Rankey (2013) highlighted that still remains unclear the details of shoals evolution through time.

On the Bahamas, ooid shoals occur along most of the platform margin. Ooid-skeletal grains with some lime mud form islands with beaches and dunes, as well as channel bars and levees within sandflats. Ball (1967) distinguished four types of carbonate sand bodies in Florida and Bahamas: marine sand belts, tidal bar belts, eolian ridges and platform interior sand blankets. Tidal-bar belts and marine sand belts respond primarily to daily tidal flows and to wave- and storm-generated currents. The internal structure of the sand blankets records the work of burrowing, where organic churning is so extensive that individual burrows are obscured; the gross setting of this sand body type is the area between the high-energy zone near the platform edge and the relatively low-energy zones at the shadows of islands (Harris, 2009).

Rankey and Reeder (2011) have recently reviewed the sand margin oolitic shoals of the Bahamas in terms of geomorphic and sedimentologic features. The building blocks of shoal complexes include: longitudinal tidal sand ridges, transverse shoulder bars, parabolic bars, and sand flats. Shoal dimensions are very variable in both width and extension, from few

to tens of kilometers along strike. For example, in the Lily Bank, a tidal-dominated active shoal, the sandy body is 4-km wide and extends over 27 km along strike.

In modern sand shoals, the vertical sequence is usually shallowing upwards, with few-meters-thick packages. The Joulters Cays sand shoal consists of a few-meters-thick coarsening-upward vertical succession of peloid wackestone at the base, fine-peloid packstone in the middle, and ooid packstone at the top (Harris, 2009). The internal structure in a marine sand belt, consist of a basal set of large- to medium-scale cross-beds overlain by small-scale cross-bed sets. Dip direction of cross-bedding indicates sand movement into the platform interior, or off bank transport if the sand shoals occur in the leeward side of an isolated oceanic bank (Hine, 1977; Hine and Neumann, 1977; Hine and Mullins, 1983). In the tidal bars the internal structure consists of a basal burrowed oolitic sand unit with an admixture of muddy pellet-ooid sediment, and an upper unit of medium- and small-scale cross-bed sets dipping perpendicularly to the bar trend (Harris, 2009).

Another important characteristic of modern ooid shoals is that they usually overlie lagoonal sediments, as result of the migration toward the inner platform in both tide- and wave-dominated sandy margin. This bank-ward progradation is easily recognizable observing the landward dipping direction of cross-beds (Gonzalez and Eberli, 1997). Where off-bank transport occurs in leeward margin or in area with tidal-ebb delta, bar foresets are instead basinward dipping, but prograded over marginal facies, or discharged directly into the slope/basin according to the adjacent physiography of the platform. Dip angle of the sand waves within the shoals is commonly higher than in the ILPWs; in the modern shoals in Lee Stocking Island they reach up to 24° (Gonzalez and Eberli, 1997).

In outcrop examples, carbonate sand shoals may extend from 1 km to 20 km. In the Triassic Muschelkalk in Germany, a gently inclined carbonate ramp filling an epicontinental basin, carbonate shoal sandbodies extend laterally for 10–20 km with very gradual changes. Aigner et al. (2007) have regarded these sand shoals as submarine barrier bars and as mobile nearshore shoal belts on local paleo-highs. There, meter-scale cycles (0.7 m to 3.5 m thick) are ubiquitous and consist of a regressive and a transgressive hemi-cycle separated by turn-around points. Major differences in character, geometry, and distribution of the sand shoals reflect the strong sensitivity to small changes in accommodation, triggered by the interaction of hierarchically organized sea-level changes with a subtle paleo-relief. At medium-scale cycles, mean thicknesses of different types of shoal bodies, range from 4.2 m for shoal bodies, to 0.3 m for skeletal

sheets, and 0.69 m for regressive oolitic shoals. The apparent layer-cake stratigraphy that appears on the kilometer to regional scale turns out to be a pseudo-layer cake, with very gentle (0.01º–0.001º dip) clinoforms organized in very subtle offlapping, pinch-out geometries (Palermo et al., 2010).

These bank-margin sands and sand shoals are abundant, sufficiently distinct and economically important as carbonate reservoir. In the Hugoton embayment of southwestern Kansas, oolitic deposits within the St. Louis Limestone have produced more than 300 million bbl of oil; these oolitic sand shoal reservoirs are relatively thin (<4 m) (Qi et al., 2007). Nevertheless, they do not represent all accumulations in the geologic record. In our case, none of the characteristics of the oolitic sand shoals can be compared with the Pozuel Formation.

6.2.- Beaches and beach ridges

Beach and beach ridges are wave-built supratidal and/or intertidal forms (Tamura, 2012; Mauz et al., 2013) also characterized by large-scale low-angle cross-beds. They are elongated sand bodies, paralleling strike direction and accreting seawards. In beaches, the width of the shoaling, surf and swash zones will depend on wave height and beach gradient (a function of sediment size and wave height), while tide range will determine the vertical stability or daily movement of all three zones (Short, 1996). In micro-tidal beach systems, the tidal range has a negligible role in determining beach morphology.

The origin of beach ridges includes progradation of sandy beach, berm and fore-dune, with stratification dipping both landwards and seawards (Tamura, 2012). Gravel or coarse shell ridges may build several meters above the level of high tide (Otvos, 2000). Clinobedded beach deposits are related to the progradation of this system and are usually dissected by erosion surfaces. In any case seaward-dipping clinobeds are usually gently dipping (less than 10º) and related to the foreshore, i.e., the zone between the high and low tide. Beach ridges form only on dissipative beaches and have a gentle gradient in the intertidal and shallow subtidal area (Davis and Fitzgerald, 2004). Individual beach ridges normally have heights on the order of a few meters and widths measured in tens of meters. Grouped in sets separated by erosion surfaces, ridge sets can extend up to several tens of kilometers along the shoreline. Dott and Mickelson (1995) reported beach ridges to be 0.5 m to 8 m high, 50 m to 200 m spaced, and subparallel to the coast.

Contrarily to sand shoals and bank-margin shoal complexes that form in shallow subtidal waters, beaches and beach ridges form in intertidal and supratidal conditions. Both systems build sedimentary bodies with large-scale low-angle cross-beds, which are elongated on strike direction and accrete seawards. Nevertheless, the beach and beach ridge lithosomes have a limited thickness constrained by the sediment size and the wave height, and in the beaches also the difference between high and low tide (Dott and Mickelson, 1995).

The oolitic clinobedded lithosomes of the Pozuel Formation share with beach and beach ridge lithosomes the along strike elongation and the seawards accretion. Nevertheless, they essentially differ in thicknesses and sedimentary structures. Beach and beach ridges are commonly up to few meters thick, deposited in intertidal and supratidal conditions. Contrarily, the Pozuel clinobedded lithosomes were deposited in subtidal conditions, prograding onto- and interfingering with basinal muds, and being the thickness of the clinobeds a function of the bathymetry of the basin. Additionally, beaches prograde over erosion surfaces: "*ravinement erosion surfaces*" if formed during transgression (Swift, 1968) or "*marine regressive surfaces of erosion*" if formed during forced regression (Dominguez and Wanless, 1991; Nummedal et al., 1993) whereas in the Pozuel clinobeds an unconformity is the upper boundary of the accretional units.

6.3.- The infralittoral prograding wedge

The oolitic and associated facies that form the Pozuel Formation, conform with the infralittoral prograding wedge (ILPW) model (*sensu* Hernández-Molina et al., 2000; Pomar and Tropeano, 2001; Fernández-Salas et al., 2003; Lobo et al., 2004, and Mateu-Vicens et al., 2008), a progradational platform-margin slope, in which topset, foreset, and bottomset beds can be recognized (**Fig. 13**). The infralittoral wedges prograde below the wave base level in wave-dominated coasts, being the upper boundary the "*ravinement surfaces*" if formed during transgression or the "*marine regressive surfaces of erosion*" if formed during regression.

The ILPW form contour-parallel elongated wedges, roughly sigmoidal in dip section, and they are the product of physical accommodation only (*sensu* Pomar and Kendall, 2008). In the Pozuel Formation, these lithosomes exhibit complex sigmoid-oblique geometries, with 5–20 m of depositional relief (thickness) of the basic accretional units and dip-oriented lengths of about 0,5–2 km. The foreset angles dip about 5º–10º and the oolitic facies occur in 50- to 70-m-thick stacks of accretional units. The coated grains were produced,

winnowed, and transported along the high-energy platform top (topsets of the wedge) before being exported seaward toward the breakpoint, where they cascaded onto the frontal slopes as sporadic grain flows or mass flows. The most conspicuous lithology is the oolitic grainstone, with muddy matrix only preserved in the toe of the slope packstones and in the inter-mound sediments in the inner part of the topsets.

Similar sedimentary wedges have been profusely described from high-resolution seismic studies from Holocene and Pleistocene deposits on modern continental shelves (**Table 2**). From those, Hernández-Molina et al. (2000) defined the "*Infralittoral Prograding Wedge,"* a narrow shore-parallel depositional body prograding below wave base. Subsequently, Fernández-Salas et al. (2003) and Lobo et al. (2004, 2005) added precision to the model. Previously, Field and Roy (1984) described these Holocene wedges and suggested the offshore transport of sediments. Chiocci and Orlando (1996) and Chiocci et al. (2004) emphasized the independence of these progradational sandbodies from sediment composition: they develop either around volcanic islands, on clastic coasts independently of riverine sediment delivery, but they can also result from carbonate production in the wave-agitated zone. From outcrop studies, Pomar and Tropeano (2001) and Mateu-Vicens et al. (2008) established in detail the process/product relationships, emphasizing 1) the predominant introduction of sediment (both *in-situ* skeletal production and lithoclastic supply) in the shoreface zone, 2) the leading effect of waves and associated currents in stirring the sediments and transferring them down the slope, and 4) the genetic relationship between the internal architecture and the changes in the base level (**Fig. 14**).

These wedges can either be laterally related to coeval deltaic deposits or they can also appear as isolated shore-parallel, seaward-prograding bodies, unconnected to any fluvial sediment source. They can also be composed by carbonate grains produced in shallow-water conditions, above the base of wave action (Mateu-Vicens et al., 2008). Accordingly, the origin of these prograding bodies was interpreted as the product of sediment reworking in the shoreface by storm waves and cross-shore sediment flux led by downwelling storm currents (Hernandez-Molina et al., 2000; Pomar and Tropeano, 2001; Lobo et al., 2005). Although the most obvious progradational configuration of the ILPWs is seawards directed, the actual sediment transport is oblique with a significant longshore component (Hernandez-Molina et al., 2000; Lobo et al., 2005).

The internal structure of ILPWs is much more complex (**Fig. 13**). When longshore currents produce significant littoral drift, the ILPWs are composed of internal shingled units, with oblique-tangential to sigmoidal reflection patterns, parallel or obliquely accreted to the main

shoreline. Major scale, alternating, progradation/aggradation segments depend on low-amplitude, sub-Milankovitch scale, sea-level fluctuations. Within these segments, changes in the magnitude and/or direction of storm events, and changes in sediment supply induced by climatic shifts, millenial to sub-millennial scale, control the internal heterogeneities (Lobo et al., 2005; Fernández-Salas et al., 2009).

For these ILPWs, Mitchel (2012) and Mitchel et al. (2012) have evidenced that the effect of gravity moves particles downslope with a flux proportional to the slope, where bed sediments are agitated by waves. The gravity effect on particles oscillated by waves or moved by along-slope currents will contribute to diffusion of the topography. Consequently, the rollover curvature (the upward convex zone between the topsets and foresets) relate to wave properties and to the offshore component of sediment flux. According to these authors, the rollover reflects a critical threshold. During quiescent conditions, sediment is likely deposited on the topset of the clinoform as well as on its foreset, and in extreme conditions sediment on some part of the foreset may become mobilized. Preservation of the topsets in the sedimentary record depends on the subsidence- and/or high-sedimentation rates preventing them from erosion either during important storms and or low-amplitude falls of sea level. Sediment below the rollover is therefore mobile during extreme wave conditions. The results provided by Mitchel (2012) and Mitchel et al. (2012) support the view that sediment is exported during energetic sea conditions from the shoreface and deposited at a depth below which the oscillating wave currents are below the threshold of motion of the sediment (Field and Roy 1984; Hernández-Molina et al. 2000).

This view is also in agreement with Peters and Loss (2012) who has recently questioned the commonly accepted concept about a distinct bimodal separation in the size of fair-weather and storm waves, and in the manifestation of such differences in stratigraphic successions. These authors have demonstrated the unimodal character of wave-size frequency distributions, as there is a continuously increasing probability for a wave to reach the bottom with decreasing water depth. And it also fully fits with the concept of “shelf equilibrium profile” (*sensu* Swift and Thorne, 1991) in controlling sediment accumulation on clastic seas.

6.4.- Wave base and the shelf equilibrium profile

Analysis of the relationships between bedding patterns, facies architecture, bounding surfaces, and sediment composition in a Plio-Pleistocene outcrop example in Matera, Italy, evidenced the effect of waves and storm-driven downwelling currents in stirring the clasts

from the shoreface zone down to the rollover, and revealed the internal architecture of the building blocks to result from changes in the base level (Pomar and Tropeano, 2001; Mateu-Vicens et al., 2008) (**Fig. 14**). During relative sea-level stillstands, some aggradation but mainly progradation occurred. Topsets accumulated under the wave action (shoreface), and sediments stirred by waves and associated currents were carried to the rollover where gravitational flux occurred, inducing the prism to prograde, as a non-regressive progradation (**Fig. 14 A**). Subsequent rise of sea level (or subsidence) allowed the topsets to be preserved due to the elevation of the "base level." Nevertheless, a subsequent fall of relative sea level induced a lowering of the base level and, consequently, erosion of the previously deposited topsets (shoreface) and the upper part of the clinobeds (**Fig. 14 B**). The increase on sediment supply during fall of relative sea level induced an internal downlap surface to form and the prism to prograde during regression. As this erosion represents a "marine regressive surface of erosion" (*sensu* Dominguez and Wanless, 1991; Nummedal et al., 1993) not subaerial exposure exists on top of the prograding prism; only the thin regressive beachface deposits formed in the landward edge has potential for subaerial exposure during fall of relative sea level (**Fig. 14**).

Contrarily to most beach-nearshore sedimentation models that consider the beachface deposits to wedge out and to evolve, seawards, into fine-grained sediments, with a decreasing signature of wave action (e.g., Swift and Thorne, 1991; Swift et al., 1991), the ILPW becomes an important depositional model for wave-dominated coasts, in which sediment supply is important and longshore currents significant to induce neat littoral sediment drift (Lobo et al., 2005; Fernández-Salas et al., 2009).

At geological scale, the shelf equilibrium profile results from a balance between sediment input and fluid power, were fluid power, a large-scale diffusion mechanism, relies on the episodic nature of transport (Pomar, 2001a). On clastic shelves, the base level for sediment accumulation tends to be the shelf equilibrium profile, a similar concept to the "wave-base" of Rich (1951), the "marine profile of equilibrium" of Dietz (1963), or the "wave-base razor" of Sonnenfeld and Cross (1993). On the shelf, sediments aggrade until they reach the level where waves and currents stir and move them; subsequently, the rates of net deposition decrease when there is sufficient fluid power to sweep sediments downshelf and offshore in response to intermittent storm and tidal currents (Swift and Thorne, 1991). These processes are episodic and produce a progressive flattening of the depositional profile, which in terrigenous systems parallels a basinward grain-size decrease (e.g., Johnson, 1919; Reineck and Singh, 1980; Allen, 1982; Swift et al. 1991) and define the "shelf equilibrium

profile" of Swift and Thorne (1991). This "shelf equilibrium profile" matches the Rich (1951) notion of "wave-base" as the greatest depth to which the bottom is stirred by waves during storms. The episodic downshelf transport results in deposition on a slope dominated by gravity processes (Swift and Thorne, 1991). Differences in the depositional profile and in the slope dip angle are related to grain size. In coarse-grained dominated systems, with low amount of fines, the depositional profile tends to have a flattened and shallower shelf surface and a steeper slope. In contrast, a fine-grained dominated system would have a flattened shoreface, a deeper position of the rollover and a gentler dipping slope (Pomar and Kendall, 2008).

Often confused with sea level, the "base level" for sediment accumulation tends to match the "shelf equilibrium profile." For coasts with high sediment supply, Fernández-Salas et al. (2009) have proven both the physical and genetic connections between prograding beach ridges and the infralittoral prograding wedges (**Fig. 15A**). Tropeano et al. (2002) already predicted this connection from a process-oriented type of analysis, by establishing (sic) "*both base levels, the sea level and the wave base level, govern sedimentary accumulation in wave-dominated shelves and, consequently, two offlap breaks may coexist (beach edge and shoreface edge) in shallow-marine depositional profile. In this setting, two seaward-clinobedded lithosomes, separated by an unconformity, may develop during relative still-stand or falls of the sea."* Latter, Fraser et al. (2005) have documented this relationship from ground-probing radar profiles across the strandplain deposits near Umiujaq, Eastern Hudson Bay, Canada. There, a bipartite shallowing-upward sandy succession formed under falling sea level, with the two-prograding units separated by a wave-erosion surface (**Fig. 15B).**

Consequently, with sufficient sediment supply and under falling sea level, the regressive beach prograding onto the ILPW has a high potential for preservation; these two clinobedded lithosomes are separated by an unconformity and the topsets may not be preserved (**Figs. 14B and 15B**). Under sea-level stillstand, topsets can be preserved and the erosion surface will be placed above the topsets and bellow the prograding beach (**Fig. 14 A and 15 A**). In this case, the infralittoral prism, with thicker clinobeds (tens of m - to more than 100 m), will be overlain by the thinner (< 10 m) cross-bedded beach lithosome and, if it is the case, by beach ridges and/or eolian deposits. In a transgressive situation, foresets and topsets will be preserved as they are placed below the base level during sea-level rise, but the retrograding beach has low preservation potential as it may be removed by erosion (ravinement) during transgression.

Thus the “shelf equilibrium profile” represents the base level for marine sediments to accumulate and defines the physical accommodation (*sensu* Pomar, 2001b; Pomar and Kendall, 2008) equivalent to the Jervey’s (1988) definition of accommodation. In this context, the space available for potential sediment accumulation (the physical accommodation) comprises the space between sea floor and the "shelf equilibrium profile" of Swift and Thorne (1991).

7. Other examples of prograding wedges: a review

Prograding prisms with architectural characteristics similar to the ILPWs are abundant in ancient carbonate platforms. Several examples have been described from both outcrops and subsurface, some of them forming good oil reservoirs. Yet interpretations in some of them may have been diverse, they share a number of characteristics with the ILPW (Pomar and Tropeano, 2001). Some differences, e.g., thickness, size and stacking patterns, can be attributed to substrate physiography, rate of sediment supply and tectonic and eustatic regimes.

- Sediment was produced/supplied within the wave-action zone, and may either be bioclastic, oolitic, peloidal, or lithoclastic derived from river input or from coastal erosion by storm waves.
- Grainstone textures, commonly well sorted, predominate, except where the clinobeds toe out asymptotically on the basinal mud (packstone to wackestones), and in the inner-platform lithofacies where low-energy facies may occur.
- These wedges are laterally extensive, parallel to the shoreline, and may be continuous over the entire shelf, as long as conditions of substrate morphology persist.
- The down-dip extent (progradation distance) is variable, being greatest where sediment supply is high.
- Thickness is variable, from few to some tens of meters, but this depends on the available accommodation space during progradation (depth of the basin), and on the vertical stacking of lithofacies (aggradation).
- Internal architecture is broadly sigmoidal to oblique; in outcrops, with topsets, foresets and bottomsets or, in seismic sections, with toplap and downlap terminations.

- Topsets deposited in shallow water, extending through the shoreface, from the shoreline down to the base of the wave action.
- The dip angle of cross-beds is also variable, but it is mostly related to grain size (angle of repose) and texture.
- Topsets are preserved when progradation occurs during a stillstand of sea level, and during elevation of the base level (transgression). But a subsequent lowering of the base level may cause erosion of the topsets.
- Microbialite, algal or metazoan mounds may occur in the topsets. Nevertheless, in-situ biota is rare in the clinobeds.

7.1.- The Upper Pliocene Capodarso calcarenite, Sicily

The Upper Pliocene Mt Capodarso Formation accumulated in the Enna–Caltanissetta piggyback basin (central Sicily) as a stack of six skeletal prograding wedges alternating with siliciclastic mudstones. These prograding wedges passes basinward into thick time-equivalent hemipelagic mudstones (Catalano et al., 1993; Vitale, 1998). Stacking patterns of the accretional units within the wedges were controlled by sea-level cycles and tectonic tilting induced by detachment folding and propagation of an underlying thrust (Lickorish and Butler, 1996; Vitale, 1998). The progressive seaward increase in thickness of the clinobedded calcarenite wedge is the result of deposition into increasingly deeper water induced by the thrust propagation.

These skeletal wedges contain topsets, foresets and bottomsets. Foresets, up to 27-m thick, extend for a few 10's km parallel to the paleo-shoreline, and 1–2 km in dip direction. They consist of well-sorted skeletal grainstones and packstones, locally rudstones, composed of benthonic foraminifers, bivalve and gastropod fragments, barnacles, brachiopods, serpulids, echinoderms, red algae and sparse bryozoans, and planktonic foraminifers. The upper boundary, commonly an erosion surface, shows no evidences of subaerial exposure.

Shingled clinobed packages with sigmoidal to oblique-tangential bedding patterns compose these wedges (**Fig. 16**). Foreset beds are decimeter thick and dip angle ranges from a few degrees up to 19º. Tectonic tilting may have induced these high dip angles (Massari and Chiocci, 2006). Clinobeds grade downdip, asymptotically, into the toesets and bottomsets, and then into terrigenous mudstones (Vitale, 1998; Massari and Chiocci, 2006).

Based on all these characteristics, Massari and Chiocci (2006) interpreted the prograding clinoforms to result from down-slope avalanche of skeletal sediments produced on and swept from the wave-dominated upper shoreface. According to these authors, the area of skeletal production was located in a storm- and wave-dominated zone, so it was a zone of bypass-erosion between the coast and the break on the slope (rollover). Deposition occurred on storm-dominated microtidal margins with long fetch. Dispersal of the skeletal components was mainly due to storm-driven downwelling and geostrophic currents that evolved into gravity flows at the slope break.

These characteristics match the attributes of the ILPW (**Table 3**). In particular, the lateral (strike) extension of the wedges, the shingling stacking of clinobed packages with oblique-tangential to sigmoidal bedding, and the few-km downdip progradation. Skeletal components dominate, and were produced within the wave-action zone (shoreface) from where swept down to the rollover by downwelling currents. Down-slope avalanche of these skeletal components induced the slope to prograde and, at the toe, to interfinger with the basinal muds.

7.2.- The Crotone Basin, southern Italy

Pleistocene prograding wedges with clinoform geometry also occur in the Crotone basin, southern Italy (Massari et al., 1999). They consist of prograding wedges deposited during regression, when the shoreline migrated downward and basinward following a low-angle trajectory induced by the syndepositional growth of gentle synclines. The sediments, with a mixed carbonate-siliciclastic composition, resulted from both carbonate production in the shoreface and high sediment delivery through short-headed, high-gradient streams from a nearby uplifting granitic massif (Massari et al., 1999).

According to Massari et al. (1999), these wedges prograded under high-energy, wave-dominated conditions; intense reworking caused by storms and the induced longshore (strike-oriented trough cross-beds) and offshore currents (offshore-directed trough cross-beds and swaley cross-beds) led to episodic down-shelf transport of sediments, which resulted on sediment shed off on a slope dominated by gravity processes (Swift and Thorne, 1991). Differences in the depositional profile and in the slope dip angle are related to grain size. It can reasonably be assumed that progradation took place from a line source and that the sand bodies are to be regarded as coastal prograding bodies.

Small sigmoidal units bounded updip by ravinement surfaces and the correlative conformity downdip compose these wedges. Within individual units, bedding patterns changes from a lower sigmoidal thin package into a thicker package with oblique-tangential, with toplap terminations. The stacking of these sigmoidal units outlines topsets, foresets and bottomsets. Topset beds (foreshore) have strike- and downdip-oriented trough cross-bedding (**Fig. 17**), planar lamination, wave megaripples, and, locally, shell pavements, indicating sediment transport was complex: longshore currents and cross-shore sediment flux led by downwelling storm currents.

Foresets consist of decimeter-thick beds of fine sand to granule, with 10º to 16º dip angles, depending on grain size. Beds are mostly planar-laminated and, locally, normal grading may occur. Rhythmic pattern is ubiquitous. Sets of scour-based backset beds do locally occur. Gravity-driven flows on the slope induced by sediment shed off from the platform top (shoreface) lead the prism to prograde below the base of wave action. Foreset beds merge asymptotically downdip into bioturbated toesets and bottomsets interbedded with bluish mud.

Despite the outcrops are limited to identify some characteristics, such as the alongshore elongation, these wedges share many others characteristics of the ILPWs (**Table 3**), namely the architectural elements and the processes involved in deposition of the sedimentary bodies.

7.3.- The Amellago ramp, Morocco

Pierre (2006) and Pierre et al. (2010) have documented in detail the facies and bedding architecture of the Aalenian/Bajocian Amellago ramp in the Central High Atlas, Morocco. This seismic-scale carbonate ramp was studied in a 37-km long and 1000-m high continuous and undeformed outcrop.

The Amellago ramp system was built by stacking of more than 25 accretional units. These accretional units are bounded by erosion surfaces in the up-dip portion that, basinward correlate and dissipate into an inconspicuous conformable bedding surface within the hemipelagic basinal marls. In the up-dip portion, the erosion surface has irregular relief, holds different encrusting biota and bivalve bored on it (hardground). It is interpreted to result from transgression onto a partially exposed platform.

The accretional units exhibit complex sigmoid-oblique geometries, and topset, foreset, and bottomset beds are well developed (**Fig. 18**). The main lithofacies is a clinobedded oolitic

grainstone, around 15–20 m thick. Above a lower oolitic aggradational interval, the oolitic belt becomes detached from the shoreline in the upper part of the unit, leaving behind a km-wide, shallow-water, inner ramp environment (Pierre et al., 2010). Sediments in this inner setting consists of bioclastic and peloidal wackestone-packstone to floatstone. Shallow-water deposits in the topsets are not clearly documented, but water depth at the breakpoint is estimated as less than 10–20 m. Offshore to the clinobedded oolitic belt, the distal ramp interfingers with marl-mud with echinoids, ostracods, bivalves, brachiopods and bryozoans. The estimated depth of this outer ramp basin ranges 40 to 60 m.

The production area of the ooids was a shallow-water narrow belt, elongated in strike direction (> 15 km) and estimated in less than 1 km wide in dip direction, although oolite progradation built out prisms of about 10–15 km wide in dip direction with up to 3–4º clinoform dip angle. The intense action of waves and tidal currents, along with the alternating high-stand and low-stand sedimentation and the abundant mud in the basin, kept low the angle of the sloping clinobeds. Pierre et al. (2010) and Christ et al. (2012) considered the Amellago ramp to be the result of two alternating carbonate systems: a muddy ooid-free ramp developed during early transgression, and an oolitic ramp during the late transgressive and highstand part of fourth-order sea-level cycles.

Independently of this interpretation, the Aalenian/Bajocian Amellago oolitic ramp also holds the attributes of the infralittoral prisms (**Table 2**). In particular, the sigmoidal and tangential-oblique internal architecture with toplap and downlap strata terminations, the along-strike elongation, the progradation direction, the grainstone-dominated texture in the upper part of the units that becomes muddier downslope where they interfinger the basinal muds. Additionally, the interpreted depositional processes are also similar to those of the ILPW, namely the production of ooids and peloids within the wave-action zone, the longshore- and cross-shore sediment flux dominating on the topsets (shoreface), and the gravity-driven flows on the slope that induced the prism to prograde below the base of wave action.

7.4.- Las Pilas Formation, Coahuila, northern México

Osleger et al. (2004) documented in detail the progradational architecture of a platform margin-slope from the exceptional exposures of the upper Albian Las Pilas Formation in El Cedral outcrop, northern Mexico. The goal was to produce an outcrop model for analogous Cretaceous reservoirs. The prograding Las Pilas clinobedded unit also holds most of the attributes of the infralittoral prisms.

The 140-m thick Las Pilas limestones at El Cedral consists of large-scale high-angle clinobeds that prograded more than 5 km (exposed width) over the basinal mudstones of the Salmon Peak Formation, during a time span approximately of 2.1 Ma. It exhibits complex sigmoid-oblique geometries, and topset, foreset, and bottomset beds are well developed.

Las Pilas clinobedded units are 40- to 60-m thick, composed by sand-sized, well-sorted, well-rounded, coated grains and skeletal fragments of shallow-water origin. The primary sediment fabrics are fine- to coarse-grained grainstones and mud-lean packstones with remarkably homogeneous lithofacies; no obvious textural or compositional difference is recognized between topset and foreset beds. Sorting ranges from good to moderate, with occasional bimodal sorting. Bottomset beds have similar composition to those of foreset beds, although grain size typically decreases, and the amount of mud increases distally.

Topset, foreset, and bottomset facies tend to be thick- to massively bedded, with subtle appearance of cross-beds as the homogeneity of the sediment inhibits the well-defined cross-stratification. Similarly, significant time-stratigraphic surfaces are difficult to recognize. Osleger et al. (2004) emphasize that given only the vertical measured sections (or core or downhole logs), it would be very difficult to correlate coeval sediment bodies, recognize clinobedded geometries and identify topsets and foresets.

The topset beds range from 5 m near the updip termination to about 35 m thick near the rollover. There, the stratal surfaces show no obvious evidence of erosional truncation, but rather merge asymptotically updip at low angles. Osleger et al. (2004) have estimated the rollover (breakpoints) of the clinobedded units to be located at less than 10–20 m of water depth. Considering the thickness of the clinobeds, Osleger et al. (2004) estimated the bathymetry at the toe of the slope to range between 50 m and 80 m.

The dip direction of clinobeds is dominantly oriented to the southwest, indicating a uniform progradation direction. In the foresets, dip angles of the master bounding surfaces range from 8º to 15º, but within the accretional units depositional dips are variable, ranging from subhorizontal to about 20º. Bottomset beds thickness varies from about 10 m to 20 m at the toe of slope, and the dip angle decreases asymptotically toward their terminus to pinch out downdip, resting on top of basinal facies rather than interfinger.

The lime sands were winnowed, coated, and micritized along the high-energy top of the clinobedded units before being exported seaward toward the breakpoint, where they cascaded down the frontal slopes. The variability in the orientations of cross-beds, suggest

a combination of longshore-, storm- and tidal currents to spread the lime sands on top of the ramp margin. Gravity-driven flows on the slope induced the prism to prograde below the base of wave action. Two mechanisms for sediment deposition have been suggested seaward of the breakpoint (Osleger et al., 2004): (1) structureless grainstones at the base of the slopes, with relatively low dip angles may have accumulated episodically by slumping and turbulent mass flows; (2) higher-angle units located along the upper slopes may have formed episodically by grain flow down the avalanche faces of steeply-dipping foresets.

All these attributes of Las Pilas Limestone in the El Cedral, are shared with the infralittoral prisms (**Table 3**) as well as the interpreted depositional processes.

7.5.- The Smackover Formation in northern Louisiana and south Arkansas

The Smackover Formation across much of the Gulf Coast basin of the USA consists of a shoaling-upward cycle, nearly 100 m thick, capped by oolitic/oncolitic packstones and grainstones. It is from where the homoclinal ramp depositional model was first conceived (Ahr, 1973). The stratigraphy, lithofacies and depositional environments of the Oxfordian Smackover Formation has long been known because of its economic importance as one of the most prolific oil and gas producing formations around the northern rim of the U.S. Gulf Coast (Heydari and Baria, 2005). Oil and gas are sourced in the organic-rich carbonates at the base of the Smackover Formation, accumulated in the permeable and porous grainstones at the top, and sealed by the anhydrite of the Buckner Formation (Heydari and Baria, 2005).

The homoclinal ramp model (Ahr, 1973) has long been a very popular hypothesis for the Oxfordian Smackover Formation. This ramp is made by a series of strike-oriented facies belts that include evaporites and red beds to the north, that passes basinward (inner ramp) into oolites (beaches and shoals), followed by peloidal lithofacies (mid-outer ramp) and laminated basinal wackestones and mudstones (Baria et al., 1982). Nevertheless, and despite the wealth of information after years of investigations, some aspects of the Smackover Formation still remain unresolved, yet its basic depositional environments are not entirely clear (Heydari and Baria, 2005).

In the north-central portion of the U.S. Gulf Coast (Mississippi, Louisiana, and Arkansas), three sequences are recognized within the Smackover Formation (**Fig. 19A**): the Smackover “C,” the Smackover “B,” and the Smackover “A” in ascending order (Heydari and Baria, 2005, 2006, 2008). These sequences are bounded by subaerially exposed

unconformities at the top, which are correlative to siliciclastic turbidites in the basin (Moore, 2001). The Smackover “C” is 183-m (600 ft) thick and best developed in the landward side of the Smackover belt. It consists of basinal lime mudstone that shoals up into ooid grainstone with a well-defined shelf margin. With a layer-cake-type stratigraphy, these ooid grainstones are not forming a single sheet but consists of numerous discrete prograding units (Heydari and Baria, 2005).

The Smackover “B” sequence is 180-m thick (600 ft) and is best developed in the middle to southern portion of the Smackover belt. Recent 3D seismic data analyses in North Louisiana and South Arkansas, have shown numerous shingled-sigmoidal clinoform strata to conform the upper part of the Smackover “B” sequence (**Fig. 19C**) over an area of around 19 km in dip direction and 32 km in strike direction (Heydari and Baria, 2005; Handford and Baria, 2007). These clinoform bodies range in thickness from 50 m to 70 m, and are around 1-km wide (600–1200 m) in dip direction (distance from toplap to downlap pinchout points) thus being significantly steep (4–7º) and narrow for being in an homoclinal-type of ramp. On strike direction, the clinoforms are elongated and remarkably continuous throughout the entire area of the 3D seismic survey; single visible clinoform extends 6–16 km in strike direction before disappearing or being truncated by a younger clinoform. Lithofacies at the updip termination of the clinoforms correspond to beach environment, foreshore to berm and possibly coastal eolian dunes, and grainy but muddy subtidal facies at the down-dip toe. Assuming the height of the clinoform units to represent the water depth, Heydari and Baria (2005) and Handford and Baria (2007) estimated water depths of 50–70 m at a distance of less than 1 km from the shoreline.

The 21-m thick (70 ft) upper Smackover “A” sequence occurs in the southernmost part of the Smackover Trend and consists of isolated lithosomes, with facies shallowing up from skeletal packstone into ooid-oncoid grainstone, and finally into ooid grainstone (Heydari and Baria, 2005).

Summarizing the basic characteristics of the Smackover sequence “B” in northern Louisiana and south Arkansas, it can also be suggested that it holds most of the attributes of the infralittoral prisms (**Table 3**): (1) internal architecture is sigmoidal with well-defined toplap and downlap surfaces; (2) grainstone textures, commonly well sorted and mud free, predominate in the upper part of the units, and muddy textures at the bottom; (3) clinoforms are laterally extensive in strike direction, paralleling the shoreline; (4) clinoforms prograde basinward with variable distance; (5) thickness depends on the bathymetry of the basin, but exceeds the thickness of the foreshore; (6) shallow-water to subaerial deposits occur on top

of the accretional units (beach and possibly coastal eolian dunes); (7) the dip angle of cross-beds is related to the angle of repose; (8) sediment (oolites) was produced within the wave-action zone.

Consequently, all these common characteristics suggest the shallowing-upward prograding clinoforms — of the Smackover "B" sequence in Northern Louisiana and Southern Arkansas — were deposited as infralittoral prisms, on which peloids, ooids and oncoids were generated in shallow-water conditions and shed downslope under the action of waves and associated currents.

7.6.- The Hanifa Formation, Saudi Arabia

The middle Oxfordian to early Kimmeridgian Hanifa Formation consists of low-energy, dark-laminated organic-rich lime muds, collected under anoxic bottom-water conditions in the intra-shelf Arabian Basin, that shallow up into two grainstone and boundstone units that conform to the Hawtah and the Ulayyah Members.

Epeirogenic downwarp during the Middle Jurassic led to the development of intra-shelf basins on the Arabian Craton (Alsharhan and Kendall, 1986; Murris, 1980). Deposition of the Hanifa occurred on a carbonate shelf that rimmed these basins following inundation by a shallow epeiric sea during the Late Jurassic (Ziegler, 2001). Clastic influx was inhibited during highstands of sea level, allowing for deposition of algal-foraminiferal wackestones and packstones and reservoir-grade oolitic and peloidal packstones and grainstones on the shallower part of the shelf. The deeper parts of the Arabian intra-shelf basin were starved and hosted anoxic marls, and kerogenous micrites and shales which formed excellent source rocks (Ayres et al., 1982; Murris, 1980).

The middle Oxfordian to early Kimmeridgian Hanifa Formation overlies an unconformity on top of the Callovian Tuwaiq Mountain Limestone. The Hanifa shelf-margin carbonates prograded, downlapping, thinning and wedging out into the argillaceous deep-water deposits of the Arabian and Rub' Al-Khali intra-shelf basins (Ziegler, 2001).

The shallow-shelf facies of the Hanifa Formation extends for some several hundreds of kilometers along the border of the Arabian intra-shelf basin (**Fig. 20**). In outcrop, the Hanifa Formation is 113- to 180-m thick (Énay et al., 1987; Vaslet et al., 1991) and consists of two 3rd-order sequences: the middle Oxfordian Hawtah Member, and the late Oxfordian to possibly early Kimmeridgian Ulayyah Member (Vaslet et al., 1991; Mattner and Al-Husseini, 2002; Al-Husseini et al., 2006; Hughes et al., 2008; Al-Husseini, 2009).

In the subsurface of the Khurais Complex area, the lime mud-rich facies of the Hawtah Member shallow up into peloidal-oolitic grainstones. These grain-dominated lithofacies occur in an elongated belt that extends at least 100 km in strike direction. Thickness of the Hawtah grainstones is variable, but ranges from 12 to 15 m (40 to 50 ft). The lower part of the grainstone lithosome is massive to planar laminated and homogeneous in terms of both grain composition and grain size. The upper part of the lithosome is heterogeneous in terms of grain sizes and marked by cross-bedded layers and some subtle bedding planes. Shallow-water components, such as miliolids, fragments of dasycladacean green algae *Pseudoclypeina sp*p. and *Clypeina jurassica,* and fragments of reworked stromatoporoids and corals occur in the upper part of the lithosomes.

The transition from the basinal mudstones to the grainstones can either be sharp or transitional. When transitional, two patterns are observed: 1) the transitional interval is made by wackestone to packstone textures grading up into the grainstones (**Fig. 21B**), or 2) the transition interval consists of thin grainstone- to mud-lean packstone layers interbedded with the lime muds (**Fig. 21C**). In any case, this sediment organization requires shedding down of sediments from the shallow- agitated water down into low-energy basin by gravity (non tractive) flows.

In most of the studied cores in the Khurais Complex, muddy- to grainy-dominated boundstone with stromatoporoids, corals and rare *Cladocoropsis* occur atop the grainstones. Thickness of this facies varies and ranges from 6 to 12 m (20 to 40 ft). Microbially induced textures in this unit are cryptic and marked by dense micrites, microbial filaments, clotted fabrics with local outward and/or upward protrusions, in addition to microbially induced peloidal clots. Locally, oncoidal rudstone/floatstone also occurs at the transition from the boundstone intervals and the overlaying muds of the Ulayyah Member.

Ulayyah basinal lime mudstones sit above the shallow-water facies of the Hawtah Member, which requires a subsequent increase of accommodation. The Ulayyah Member also shallows upward into microbially-bound stromatoporoid-coral buildups, deposited above the chlorocline (*sensu*, Liebau, 1984), as indicated by the presence of green algae *Thaumatoporella*. Locally, the microbial bioherms shallow up into peloidal-foraminiferal grain-dominated packstones that are terminated by an unconformity. This unconformity represents a late Oxfordian-Kimmeridgian 1.5-Myr hiatus, overlain by the basinal lime mudstones of the Jubaila Formation.

Interpreting the facies architecture and inferring the depositional model for the Hawtah's grainstone lithosomes bear a degree of uncertainty when using core well data only. Nevertheless, the comparison with the examples provided here, evidences analogies with ILPWs. The base of Hawtah grainstones interfingers the muddy basinal deposits. Despite the fact that clinobeds are not discernable from core data, the interfingering of mud-lean shallow-water deposits with basinal muds reveals gravitative transport of shallow-water components below the base of wave action, which is characteristic in ILPWs. The lower homogeneous grainstone interval holds similarities and is interpreted to represent the progradational foresets, whereas occurrence of grain- and bedding heterogeneities up-section may well be an expression of variable transport processes on the shoreface, thus characterizing topsets. Like in Frías de Albarracín (**Figs. 5, 7 and 9**), stromatoporoids and microbial-coral-stromatoporoid bioherms do occur in shallow-water conditions, at the inner part of the shoreface (topsets). Oncoidal rudstone and/or floatstone commonly occur above the microbial biostromes (**Fig. 21**), and were likely formed at the beginning of the subsequent transgression that submerged the Hawtah grainstone wedge.

Higher in the section, a new horizon of microbial-coral-stromatoporoids (Ulayyah) with no significant contribution of peloids and ooids developed as accommodation was progressively filled. This may suggest that, preceding the 1.5-Myr-long late Oxfordian-Kimmeridgian hiatus, the connection with open marine areas became reduced, causing turbulence and currents energy on the platform margin to decrease, which could have inhibited the growth of ooids and pellet formation.

8. Concluding remarks

Large-scale cross-bedded, strike-elongated sand bodies, prograding seawards on basinal muds are common in both lithoclastic and carbonate systems. Multiple models exist to explain the origin and characteristics of these grain-dominated lithosomes, most of them stressing the diversity in both location of the sediment source and type of sediments, to understand the processes controlling sand accumulation.

Bank-margin carbonate sands occur repeatedly throughout the geologic record and are prominent elements of carbonate facies models. The modern *sand shoals* and *bank-margin shoal complexes* in South Florida and the Bahamas are very well known and they are often used to interpret the distribution and composition of ancient grain-supported carbonate deposits, even in cases where differences are notable. *Beach* and *beach ridges* are also wave-built lithosomes characterized by large-scale low-angle cross-beds, elongated on

strike direction and accreting seawards. Contrarily to sand shoals and bank-margin shoal complexes that form in shallow subtidal waters, beaches and beach ridges form in intertidal and supratidal conditions. Nevertheless, the difference between high and low tide constrain the thicknesses of the beach lithosomes, and sediment size and wave height limits the thicknesses of the beach ridges.

Contrarily to sand shoals, bank-margin carbonate sands, beaches and beach ridges that form lithosomes with limited thickness above the base of wave action, the oolitic clinobedded lithosomes of the Pozuel Formation essentially differ in the thickness, in the sedimentary structures and in depositional setting. Also differences exist on the bounding surfaces; the upper boundary of these prisms is an erosion surface and the base is a downlap surface over basinal muds. In contrast, beaches prograde over erosion surfaces (**see Fig. 14**): the "*ravinement erosion surfaces*" if formed during transgression (Swift, 1968) and the "*marine regressive surfaces of erosion*" due to wave erosion during regression (Dominguez and Wanless, 1991; Nummedal et al., 1993), and beach-ridges accrete over the beach.

Large-scale grainstone wedges prograding below wave base similar to the Pozuel oolitic lithosomes, exhibiting complex sigmoid-oblique geometries, are very common in the sedimentary record. These lithosomes conform with the *infralittoral prograding wedge* (ILPW) model (*sensu* Hernández-Molina et al., 2000). Defined from high-resolution seismic lines from Holocene and Upper Pleistocene deposits on the continental shelf, the internal architecture is broadly sigmoidal to oblique, with topsets, foresets and bottomsets. Yet interpretations in some of these seismic examples may have been diverse, they share a number of characteristics with the clinobedded prograding prisms.

They are composed by fine- to coarse sand-sized, well-sorted, well-rounded grains of shallow-water origin **(Fig. 22)**. Fabrics are grainstones and mud-lean packstones with remarkably homogeneous lithology. These wedges prograded seaward onto basinal muds, with thicknesses being in the range of several 10’s of meters, depending on the bathymetry of the basin.

The ILPWs are laterally extensive in strike direction, and accumulated where a high rate of sediment production took place in shallow-water wave-dominated conditions. There, the lime sands were winnowed along the high-energy top of the clinobedded units. Orientations of cross-beds indicate a combination of longshore-, storm- and tidal currents to spread the lime sands on top of the platform until they reached the breakpoint.

Breakpoints of the clinobedded units (rollover) were commonly located a very few 10's of meters of water depth, from where the sediments cascaded down the frontal slopes and gravity-driven flows induced the prism to prograde. In the foresets, dip angles are variable, but mostly related to grain size (angle of repose). Nevertheless, in many of these wedges, sediment fabric homogeneity inhibits appearance of significant surfaces and sedimentary structures are difficult to recognize.

Among ILPWs, differences in thickness, size and stacking patterns of the basic accretional units, can be attributed to substrate physiography, rate of sediment supply and tectonic and eustatic regimes. But there are other important differences such as in the composition of grains. These differences derive from the type of the carbonate factories, which may change through time (e.g., Pomar and Hallock, 2008), with latitude, and also induced by differences in paleoceanographic conditions between basins.

Three main compositional groups of grains can be considered to reflect the major changes in carbonate factories through the Mesozoic and Cenozoic (e.g., Pomar and Hallock, 2008) (**Fig. 22**). The *Jurassic*, a period with significant "biologically-induced carbonate precipitation" (Pomar and Hallock, 2008) was a time for oolites, peloids and microbialites, where Mg/Ca ratio in seawater (Stanley and Hardie, 1998, 1999) might have controlled the occurrence of aragonite-facilitating or aragonite-inhibiting episodes, (Sandberg, 1983). Thus, stromatoporoids and microbial bioherms colonized the inner part of the platform top (topset beds) in the Pozuel example whereas ooids dominated the outer part.

The onset of the skeletal factory by the middle *Cretaceous* coincides with the peak in absolute Ca^{2+} concentration that promoted biotically-controlled calcification (Pomar and Hallock, 2008). Carbonate production was characterized by massive calcification of thick-shelled rudists along with an increase in abundance of calcareous phytoplankton and planktonic foraminifers. Cretaceous ILPWs were either dominated by ooids (e.g., Las Pilas; Osleger et al., 2004) or by skeletal grains (e.g., Santonian, Vilanoveta, Spain; Pomar et al., 2005).

Major changes of the skeletal factory through the *Cenozoic* can be seen as adaptations to decreasing Ca^{2+} and pCO^2, rising Mg/Ca ratios, changes in global temperature and in latitudinal and bathymetric temperature gradients (Pomar and Hallock, 2008). The large benthic foraminifera (LBF) dominated carbonate ramps during the Late Paleocene to Late Eocene thermal optimum interval; as carbonate production mostly occurred down in the oligophotic zone, below surface waves action, transport and accumulation was triggered by

other processes (e.g., internal waves, Mateu-Vicens et al., 2002), which prevented the formation of ILPWs. But progressive increase of carbonate production by seagrass epiphytic biotas in the shallow, euphotic zone during the Oligo-Miocene, and especially the Pliocene, favored the formation of ILPWs, such as the Capodarso calcarenite.

9. Final conclusion

Last but not least, we underline that the *infralittoral prograding wedge* model here applied to the Pozuel Formation, along with the comparative analysis of other Cenozoic and Mesozoic reviewed examples, can also be broadly applied to other prograding grain-dominated lithosomes, being some of them significant hydrocarbon reservoirs. The *infralittoral prograding wedge* (ILPW) may provide a satisfactory alternative model for grainstone-dominated lithosomes accumulated below wave base that not conform the traditional *sand shoal models* constructed from observations in the Recent classical localities of South Florida and the Bahamas.

Acknowledgments

We would like to thank Saudi Aramco for granting permission to publish data from the Hanifa Formation, Saudi Arabia. Our appreciation is also extended to Larry Baria and Jura-Search Inc. (Jackson, MS, US) for providing seismic and log data from the Smackover Formation. Funding was provided by Spanish Project CGL2009-13254 (to L.P. & M.M) and Aragon Government Project H54 Research Group (to B.B. and M.A.).

References

Ahr, W.M., 1973. The carbonate ramp- an alternative to the shelf model. GCAGS Transactions 23, 221–225.

Aigner, T., Braun, S., Palermo, D., Blendinger, W., 2007. 3-D geological modeling of a carbonate shoal complex: Reservoir analog study using outcrop analogs. First Break 25, 65–72.

Al-Husseini, M.I., 2009. Update to Late Triassic – Jurassic stratigraphy of Saudi Arabia for the Middle East Geologic Time Scale. GeoArabia 14, 145–186.

Al-Husseini, M. I., Matthews, R. K., Mattner, J. (2006). Stratigraphic note: Orbital forcing calibration of the Late Jurassic (Oxfordian–early Kimmeridgian) Hanifa Formation, Saudi Arabia. GeoArabia 11, 145–9.

Allen, J.R.L., 1982. Storm sequences in shallow water, in: Allen, J.R.L. (Ed.), Sedimentary structures: their character and physical basis, Developments in Sedimentology, 30B. Elsevier, Amsterdam, Oxford, New York, pp. 471–506.

Alsharhan, A. S., Kendall, C.G.S.C., 1986. Precambrian to Jurassic rocks of Arabian Gulf and adjacent areas: Their facies, depositional setting, and hydrocarbon habitat. AAPG Bull. 70(8), 977–1002.

Aurell, M., Bádenas, B., Bosence, D.W.J., Waltham, D.A., 1998. Carbonate production and

offshore transport on a Late Jurassic carbonate ramp (Kimmeridgian, Iberian basin, NE Spain): evidence from outcrops and computer modelling, in: Wright, V.P., Burchette, T.P. (Eds.), Carbonate Ramps. Geol. Soc. London Spec. Public. 149, pp. 137–161.

Aurell, M., Robles, S., Bádenas, B., Quesada, S., Rosales, I., Meléndez, G., García-Ramos, J.C., 2003. Transgressive/regressive cycles and Jurassic paleogeography of Northeast Iberia. Sediment. Geol. 162, 239–271. doi:10.1016/S0037-0738(03)00154-4

Ayres, M. G., Bilal, M., Jones, R. W., Slentz, L. W., Tartir, M., Wilson, A. O., 1982. Hydrocarbon habitat in main producing areas, Saudi Arabia. AAPG Bulletin 66, 1–9.

Bádenas, B., Aurell, M., 2001. Kimmeridgian paleogeography and basin evolution of northeastern Iberia. Palaeogeogr. Palaeoclimatol. Palaeoecol. 168, 291–310. doi:10.1016/S0031-0182(01)00204-8

Bádenas, B., Aurell, M., 2010. Facies models of a shallow-water carbonate ramp based on distribution of non-skeletal grains (Kimmeridgian, Spain). Facies 56, 89–110. doi:10.1007/s10347-009-0199-z

Ball, M.M., 1967. Carbonate sand bodies of Florida and the Bahamas. J. Sediment. Petrol. 37, 556–591.

Baria, L.R., Stoudt, D.L., Harris, P.M., Crevello, P.D., 1982. Upper Jurassic Reefs of Smackover Formation, United States Gulf Coast. AAPG Bull. 66, 1449–1482.

Bosence, D.W.J., 2005. A genetic classification of carbonate platforms based on their basinal and tectonic settings in the Cenozoic. Sediment. Geol. 175, 49–72. doi:10.1016/j.sedgeo.2004.12.030

Catalano, R., Di Stefano, E., Nigro, F., Vitale, F.P., 1993. Sicily mainland and its offshore: a structural comparison, in: Max, M.D., Colantoni, P. (Eds.), Geological Development of the Sicilian–Tunisian Platform, Unesco Report in Marine Science 58, pp. 19–24.

Chiocci, F.L., Orlando, L., 1996. Lowstand terraces on Tyrrhenian Sea steep continental slope. Mar. Geol. 134, 127–143. doi:10.1016/0025-3227(96)00023-0

Chiocci, F.L., D'Angelo, S., Romagnoli, C., 2004. Atlante dei terrazi depositionali sommersi lungo le coste italiane. Memorie Descrittive della Carta Geologica d'Italia, 58.

Christ, N., Immenhauser, A., Amour, F. Mutti, M., Tomás, S., Agar, S.M., Alway, R., Kabiri, L., 2012. Characterization and interpretation of discontinuity surfaces in a Jurassic ramp setting (High Atlas, Morocco). Sedimentology 59, 249–290. doi: 10.1111/j.1365-3091.2011.01251.x

Davis Jr., R.A., Fitzgerald, D.M., 2004. Beaches and Coasts, Blackwell Science Ltd. Malden, Massachusetts, 419 p.

Dercourt, J., Ricou, L.E., Vrielynck, B., 1993. Atlas Tethys Palaeoenvironmental Maps, BEICIP-FRANLAB, Gauthier-Vollars, Paris, 260 p, 14 maps.

Dietz, R.S., 1963. Wave-base, marine profile of equilibrium, and wave-built terraces: A critical appraisal. Geol. Soc. Am. Bull. 74, 971–990.

Dominguez, J.M.L., Wanless, H.R., 1991. Facies architecture of a falling sea-level strandplain, Doce River coast, Brazil, in: Swift, D.J.P., Oertel, G.F., Tillman, R.W., Thorne, J.A. (Eds.), Shelf sand and sandstone bodies, IAS Spec. Public. 14, pp. 259–281.

Dott, E.R., Mickelson, D.M., 1995. Lake Michigan water levels and the development of Holocene beach-ridge complexes at Two Rivers, Wisconsin: stratigraphic, geomorphic, and radiocarbon evidence. Geol. Soc. Amer. Bull. 107, 286–296. doi: 10.1130/0016-7606(1995)107<0286:*LM WATT*>2.3.CO;2

Enay, R., Le Nindre, Y.M., Mangold, C., Manivit, J., Vaslet, D. 1987. Le Jurassique d'Arabie

Saoudite Centrale: nouvelles donnes sur la lithostratigraphie, les paléoenvironnements, les faunes d'ammonites, les âges et les corrélations, in: Enay, R. (Ed.), Le Jurassique d'Arabie Saoudite Centrale, *Geobios, Mémoire Spécial* 9, pp. 13–65.

Fernandez-Salas, L.M., Dabrio, C.J., Goy, J.L., Diaz del Rio, V., Zazo, C., Lobo, F.J., Sanz, J.L., Lario, J., 2009. Land-sea correlation between Late Holocene coastal and infralittoral deposits in the SE Iberian Peninsula (Western Mediterranean). Geomorphology 104, 4–11. doi:10.1016/j.geomorph.2008.05.013

Fernández-Salas, L.M., Lobo, F.J., Hernández-Molina, F.J., Somoza, L., Rodero, J., Rodero, J., Díaz del Río, V, Maldonado, A., 2003. High-resolution architecture of late Holocene highstand prodeltaic deposits from southern Spain: the imprint of high-frequency climatic and relative sea-level changes. Cont. Shelf Res. 23, 1037–1054. doi:10.1016/S0278-4343(03)00120-1

Fezer, R., 1988, Die oberjurassische karbonatische Regressionsfazies im südwestlichen Keltiberikum zwischen Griegos und Aras de Alpuente (Prov. Teruel, Cuenca, Valencia, Spanien). Arb Institut für Geologie und Paläontologie Universität Stuttgart 84, 1–119.

Field, M.E., Roy, P.S., 1984. Offshore transport and sand-body formation: evidence from a steep, high-energy shoreface, southeastern Australia. J. Sediment. Petrol. 54, 1292–1302. doi:10.1306/212F85C1-2B24-11D7-8648000102C1865D

Fraser, C., Hill, P.R., Allard, M., 2005. Morphology and facies architecture of a falling sea level strandplain, Umiujaq, Hudson Bay, Canada. Sedimentology 52, 141–160. doi: 10.1111/j.1365-3091.2004.00680.x

Gonzalez, R., Eberli, G.P., 1997. Sediment transport and bedforms in a carbonate tidal inlet; Lee Stocking Island, Exumas, Bahamas. Sedimentology 44 (6), 1015–1030. doi: 10.1046/j.1365-3091.1997.d01-59.x

Halley, R.B., Harris, P.M., Hine, A.C., 1983. Bank Margin Environments, in Scholle, P. A., Bebout, D.G., Moore, C.H. (Eds.), Carbonate Depositional Environments, AAPG Mem. 33, pp. 463–506.

Handford, C.R., Baria, L.R., 2007. Geometry and seismic geomorphology of carbonate shoreface clinoforms, Jurassic Smackover Formation, north Louisiana. Geol. Soc. London Spec. Public. 277 (1), pp. 171–185.

Harris, P.M., 2009. Depositional Environments of Carbonate Platforms. Search and Discovery Article #60032.

Hernández-Molina, F.J., Fernández-Salas, L.M., Lobo, F., Somoza, L., Díaz-del-Rio, V., Alveirinho Dias, J.M., 2000. The infralittoral prograding wedge: a new large-scale progradational sedimentary body in shallow marine environments. Geo-Mar. Lett. 20, 109–117. doi: 10.1007/s003670000040

Heydari, E., Baria, L.R., 2005. A Conceptual Model for the Sequence Stratigraphy of the Smackover Formation in North-Central U.S. Gulf Coast. GCAGS Transactions 55, 321–340.

Heydari, E., Baria, L.R., 2006. Sequence stratigraphy of the Smackover Formation in the north-central U.S. Gulf Coast. GCAGS Transactions 56, 291–297.

Heydari, E., Baria, L.R., 2008. A regional erosional surface and its effect on the Smackover reservoir – seal system, south Arkansas – north Louisiana. GCAGS Transactions 58, 381–395.

Hine, A.C., 1977. Lily Bank, Bahamas: history of an active oolite sand shoal. J. Sediment. Petrol. 47, 1554–1581. doi:10.1306/212F73B5-2B24-11D7-8648000102C1865D

Hine, A.C., Neumann, A.C., 1977. Shallow carbonate-bank margin growth and structure,

Little Bahama Bank, Bahamas. AAPG Bull. 61, 376–406.

Hine, A. C., Mullins, H.T., 1983. The carbonate shelf-slope break, in: Stanley, D.J., Moore, G.T. (Eds.), The Shelf-break: Critical Interface on Continental Margins, SEPM Spec. Public. 33, pp. 169–183.

Hughes, G. W., Varol, O., Hooker, N. P., Énay, R., 2008. New aspects of Saudi Arabian Jurassic biostratigraphy. GeoArabia 13, 174.

Jervey, M.T., 1988. Quantitative geological modelling of siliciclastic rock sequences and their seismic expression, in: Wilgus, C.K., Hastings, B.S., Kendall, C.G.S., Posamentier, H.W., Ross, C.A., Van Wagoner, J.C. (Eds.), Sea-Level Changes: an Integrated Approach, SEPM Spec. Public. 42, pp. 47–69.

Johnson, D.W., 1919. Shore processes and shoreline development, firts ed., Wiley, New York, 584 p.

Lickorish, W.H., Butler, R.W.H., 1996. Fold amplification and parasequence stacking patterns in syntectonic shoreface carbonates. Geol. Soc. Am. Bull. 108, 966–977. doi: 10.1130/0016-7606(1996)108<0966:FAAPSP>2.3.CO;2

Liebau, A., 1984. Grundlagen der Ökobathymetrie. Paläontologische Kursbücher 2, 149–184.

Lobo, F.J., Fernandez-Salas, L.M., Hernandez-Molina, F.J., Gonzalez, R., Dias, J.M.A., Diaz del Rio, V., Somoza, L., 2005. Holocene highstand deposits in the Gulf of Cadiz, SW Iberian Peninsula: A high-resolution record of hierarchical environmental changes. Mar. Geol. 219, 109–131. doi:10.1016/j.margeo.2005.06.005

Lobo, F.J., Sanchez, R., Gonzalez, R., Dias, J.M.A., Hernandez-Molina, F.J., Fernandez-Salas, L.M., Diaz del Rio, V., Mendes, I., 2004. Contrasting styles of the Holocene highstand sedimentation and sediment dispersal systems in the northern shelf of the Gulf of Cadiz. Cont. Shelf Res. 24, 461–482. doi:10.1016/j.csr.2003.12.003

Massari, F., Chiocci, F., 2006. Biocalcarenite and mixed-cool water prograding bodies of the Mediterranean Pliocene and Pleistocene: architecture, depositional setting and forcing factors, in: Pedley, H.M., Carannante, G. (Eds.), Cool-Water Carbonates: Depositional Systems and Palaeoenvironmental Controls, Geol. Soc. London Spec. Public. 255, pp. 95–120.

Massari, F., Sgavetti, M., Rio, D., D'Alessandro, A., Prosser, G., 1999. Composite sedimentary record of falling stages of Pleistocene glacio-eustatic cycles in a shelf setting (Crotone basin, south Italy). Sediment. Geol. 127, 85–110. doi:10.1016/S0037-0738(99)00025-1

Mateu-Vicens, G., Pomar, L., Tropeano, M., 2008. Architectural complexity of a carbonate transgressive systems tract induced by basement physiography. Sedimentology 55, 1815–1848. doi: 10.1111/j.1365-3091.2008.00968.x

Mattner, J., Al-Husseini, M.I., 2002. Essay: applied cyclo-stratigraphy for the Middle East E&P industry. GeoArabia 7, 734–744.

Mauz, B., Hijma, M.P., Amorosi, A., Porat, N., Galili, E., Bloemendal, J., 2013. Aeolian beach ridges and their significance for climate and sea level: Concept and insight from the Levant coast (East Mediterranean). Earth Sci. Rev. 121, 31–54. doi:10.1016/j.earscirev.2013.03.003

Mitchell, N.C., 2012. Modeling The Rollovers of Sandy Clinoforms from the Gravity Effect On Wave-Agitated Sand. J. Sediment. Res. 82, 464–468. doi:10.2110/jsr.2012.48

Mitchell, N.C., Masselink, G., Huthnance, J.M., Fernandez-Salas, L.M., Lobo, F.J., 2012. Depths of Modern Coastal Sand Clinoforms. J. Sediment. Res. 82, 469–481. doi:10.2110/jsr.2012.40

Moore, C.H., 2001, Carbonate reservoirs. Porosity evolution and diagenesis in a sequence stratigraphic framework, Developments in Sedimentology, Volume 55: Amsterdam, Elsevier, p. 355-372.

Murris, R.J., 1980. Middle East: Stratigraphic evolution and oil habitat. AAPG Bulletin, 64, 597–618.

Mutti, M., Hallock, P., 2003. Carbonate systems along nutrients and temperature gradients: some sedimentological and geochemical constraints. Int. J. Earth Sci. (Geol. Rundsch.) 92, 465–475. doi:10.1007/s00531-003-0350-y

Nummedal, D., 1991. Shallow marine storm sedimentation - the oceanographic perspective, in: Einsele, G., Ricken, W., Seilacher, A. (Eds.), Cycles and events in stratigraphy, Springer Verlag, Berlin, pp. 227–248.

Nummedal, D., Riley, G.W., Templet, P.L., 1993. High-resolution sequence architecture: a chronostratigraphic model based on equilibrium profile studies, in: Posamentier, H.W., Summerhayes, C.P., Haq, B.U., Allen, G.P. (Eds.), Sequence stratigraphy and facies association, IAS Spec. Public. 18, 55–68.

Osete, M.L., Gómez, J.J., Pavón-Carrasco, F.J., Villalaín, J.J., Palencia-Ortas, A., Ruiz-Martínez, V.C., Heller, F., 2011. The evolution of Iberia during the Jurassic from palaeomagnetic data. Tectonophysics 502, 105–120. doi:10.1016/j.tecto.2010.05.025

Osleger, D.A., Barnaby, R.J., Kerans, C., 2004. A laterally accreting grainstone margin from the Albian of northern Mexico: Outcrop model for Cretaceous reservoirs, in: Grammer, G.M., Harris, P.M., Eberli, G.P. (Eds.), Integration of outcrop and modern analogs in reservoir modeling, AAPG Mem. 80, pp. 93–107.

Otvos, E.G., 2000. Beach ridges—definitions and significance. Geomorphology 32, 83–108. doi:10.1016/S0169-555X(99)00075-6

Palermo, D., Aigner, T., Nardon, S., Blendinger, W., 2010. Three-dimensional facies modeling of carbonate sand bodies: Outcrop analog study in an epicontinental basin (Triassic, southwest Germany). AAPG Bull. 94, 475–512. doi:10.1306/08180908168

Peters, S.E., Loss, D.P., 2012. Storm and fair-weather wave base: A relevant distinction? Geology 40, 511–514. doi:10.1130/G32791.1

Pierre, A., 2006. Un analogue de terrain pour les rampes oolitiques anciennes. Un affleurement continu à l'échele de la sismique (falaises jurassiques d'Amellago, Haut Atlas, Maroc), PhD. Thesis, Université de Bourgogne, 232 p.

Pierre, A., Durlet, C., Razin, P., Chellai, E.H., 2010. Spatial and temporal distribution of ooids along a Jurassic carbonate ramp: Amellago outcrop transect, High-Atlas, Morocco, in: Van Buchem, F.S.P., Gerdes, K., Esteban, M. (Eds.), Mesozoic and Cenozoic carbonate systems of the Mediterranean and the Middle East - stratigraphic and diagenetic reference models, Geol. Soc. London Spec. Public. 329, pp. 65–88.

Plint, A.G., 1988. Sharp-based shoreface sequences and "offshore bars" in the Cardium Formation of Alberta: their relationship to relative changes in sea level, in: Wilgus, C.K., Hasting, B.S., Kendall, C.G.S.C., Posamentier, H.W., Ross, C.A., Van Wagoner, J.C. (Eds.), Sea-level changes: an integrated approach, SEMP Spec. Public. 42, pp. 357–370.

Pomar, L., 2001a. Types of carbonate platforms, a genetic approach. Basin Res. 13, 313–334. doi: 10.1046/j.0950-091x.2001.00152.x

Pomar, L., 2001b. Ecological control of sedimentary accommodation: evolution from a carbonate ramp to rimmed shelf, Upper Miocene, Balearic Islands. Palaeogeogr. Palaeoclimatol. Palaeoecol. 175, 249–272. doi:10.1016/S0031-0182(01)00375-3

Pomar, L., Gili, E., Obrador, A., Ward, W.C., 2005. Facies architecture and high-resolution sequence stratigraphy of an upper Cretaceous platform margin succession, Southern Central Pyrenees, Spain. Sediment. Geol. 175, 339–365. doi:10.1016/j.sedgeo.2004.11.009

Pomar, L., Hallock, P., 2008. Carbonate Factories: A Conundrum in Sedimentary Geology. Earth Sci. Rev. 87, 134–169. doi:10.1016/j.earscirev.2007.12.002

Pomar, L., Kendall, C.G.S.C., 2008. Architecture of carbonate platforms: A response to hydrodynamics and evolving ecology, in: Lukasik, J., Simo, A. (Eds.), Controls on Carbonate Platform and Reef Development, SEPM Spec. Public. 89, pp. 187–216.

Pomar, L., Tropeano, M., 2001. The “Calcarenite di Gravina” Fm. In Matera (Southern Italy): new insights for large-scale cross-bedded sandbodies encased in offshore deposits. AAPG Bull. 84, 661–689.

Purkis, S., Kerr, J., Dempsey, A., Calhoun, A., Metsamaa, L, Riegl, B., Kourafalou, V., Bruckner, A., Renaud, P., 2014. Large-scale carbonate platform development of Cay Sal Bank, Bahamas, and implications for associated reef geomorphology: Geomorphology 222, 25–38. doi:10.1016/j.geomorph.2014.03.004

Qi, L., Carr, T.R., Goldstein, R.H., 2007. Geostatistical three-dimensional modeling of oolite shoals, St. Louis Limestone, southwest Kansas. AAPG Bull. 91, 69–96.

Rankey, E.C., Reeder, S.L., 2011. Holocene Oolitic Marine Sand Complexes of the Bahamas. J. Sediment. Res. 81, 97–117. doi:10.2110/jsr.2011.10

Rankey, E.C., Riegl, B., Steffen, K., 2006. Form, function and feedbacks in a tidally dominated ooid shoal, Bahamas. Sedimentology 53, 1191–1210. doi: 10.1111/j.1365-3091.2006.00807.x

Read, J.F., 1998. Phanerozoic carbonate ramps from greenhouse, transitional and ice-house worlds: clues from field and modelling studies, in: Wright, V.P., Burchette, T.P. (Eds.), Carbonate Ramps, Geol. Soc. London Spec. Public. 149, pp. 107–135.

Reineck, H.E., Singh, I.B., 1980. Depositional Sedimentary Environments, Springer-Verlag, Berlin, Heidelberg, New York, 549 pp.

Rich, J.L., 1951. Three critical environments of deposition and criteria for recognition of rocks deposited in each of them. Geol. Soc. Am. Bull. 62, 1–20.

Sandberg, P.A., 1983. An oscillating trend in Phanerozoic non-skeletal carbonate mineralogy. Nature 305,19–22. doi:10.1038/305019a0

Short, A.D., 1996. The role of wave height, period, slope, tide range and embaymentisation in beach classifications: a review. Revista Chilena de Historia Natural 69, 589-604.

Sonnenfeld, M.D., Cross, T.A., 1993. Volumetric partitioning and facies differentiation within the Permian Upper San Andres Formation of Last Chance Canyon, Guadalupe Mountains, New Mexico, in: Loucks, B., Sarg, R.J. (Eds.), Carbonate Sequence Stratigraphy: Recent Developments and Applications, AAPG Mem. 57, pp. 435–474.

Sparks, A.G., Rankey, E.C., 2013. Relations between geomorphic form and sedimentologic-stratigraphic variability: Holocene ooid sand shoal, Lily Bank, Bahamas. AAPG Bull. 97, 61–85. doi:10.1306/05101211125

Stanley, S. M., Hardie, L. A., 1998. Secular oscillations in the carbonate mineralogy of reef-building and sediment-producing organisms driven by tectonically forced shifts in seawater chemistry. Palaeogeography, Palaeoclimatology, Palaeoecology, 144, 3-19.

Stanley, S. M., Hardie, L. A., 1999. Hypercalcification: Paleontology links plate tectonics and geochemistry to Sedimentology. GSA Today, 9, 2-7.

Swift, D.J.P., 1968. Coastal erosion and transgressive stratigraphy. J. Geol. 76, 444–456.

Swift, D.J.P., Thorne, J.A., 1991. Sedimentation on continental margins, I: a general model for shelf sedimentation, in: Swift, D.J.P., Oertel, G.F., Tillman, R.W., Thorne, J.A. (Eds.), Shelf sand and sandstone bodies, IAS Spec. Public. 14, pp. 3–31.

Swift, D.J.P., Niedoroda, A.W., Vincent, C.E., and Hopkins, T.S., 1985. Barrier island evolution, middle Atlantic shelf, U.S.A. Part I: shoreface dynamics. Mar. Geol. 63, 331–361. doi:10.1016/0025-3227(85)90089-1

Swift, D.J.P., Phillips, S., Thorne, J.A., 1991. Sedimentation on continental margins, VI: lithofacies and depositional systems, in: Swift, D.J.P., Oertel, G.F., Tillman, R.W., Thorne, J.A. (Eds.), Shelf sand and sandstone bodies, IAS Spec. Public. 14, pp. 89–152.

Tamura, T., 2012. Beach ridges and prograded beach deposits as palaeoenvironment records. Earth Sci. Rev. 114, 279–297. doi:10.1016/j.earscirev.2012.06.004

Tesson, M., Allen, G.P., Ravenne, C., 1993. Late Pleistocene shelf-perched lowstands wedges on the Rhône continental shelf, in: Summerhayes, C.P., Haq, B.U., Allen, G.P. (Eds.), Sequence Stratigraphy and Facies Associations, IAS Sep. Public. 18, pp. 183–196.

Trincardi, F., Field, M.E., 1991. Geometry, lateral variation, and preservation of downlapping regressive shelf deposits: eastern Tyrrhenian sea margin, Italy. J. Sediment. Petrol. 61, 775–790. doi:10.1306/D42677D0-2B26-11D7-8648000102C1865D

Tropeano, M., Pieri, P., Pomar, L., Sabato, L., 2002. The Offlap Break Position Vs Sea Level: A Discussion. Proceedings EGS XXVII General Assembly, Nice, Volume abstract #296.

Vaslet, D., Al-Muallem, M.S., Maddeh, S.S., Brosse, J.M., Fourniquet, J., Breton, J.-P., Le Nindre, Y.M., 1991. Explanatory notes to the geologic map of the Ar Riyad Quadrangle, Sheet 24 I, Kingdom of Saudi Arabia. Saudi Arabian Deputy Ministry for Mineral Resources, Jeddah, Geosciences Map, GM-121, 1–54.

Vitale, F.P., 1998. Stacking pattern and tectonics: field evidence from Pliocene growth folds of Sicily (central Mediterranean) Plio-Pleistocene record, in: De Graciansky, P.-C., Hardenbol, J., Jacquin, T., Vail, P.R. (Eds.), Mesozoic–Cenozoic sequence stratigraphy of European Basins, SEPM Spec. Public. 60, pp. 181–199.

Westphal, H., Halfar, J., Freiwald, A., 2010. Heterozoan carbonates in subtropical to tropical settings in the present and past. Int. J. Earth Sci. 99, 153–169.doi: 10.1007/s00531-010-0563-9

Ziegler, M.A., 2001. Late Permian to Holocene Paleofacies evolution of the Arabian plate and its hydrocarbon occurrences. GeoArabia 6, 445–504.

FIGURE CAPTIONS

Fig. 1. (A) Kimmeridgian outcrops west of Teruel, central part of the Iberian Range, and location of the studied localities between the villages of Frías de Albarracín and Moscardón. **(B)** Palaeogeography of Western Europe during the early Kimmeridgian (modified from Dercourt et al., 1993). **(C)** Synthetic stratigraphy of the Kimmeridgian in the central part of the Iberian Basin. Dashed rectangle denotes the stratigraphic interval studied here (adapted from Bádenas and Aurell, 2010).

Fig. 2. (A) Marls and intercalated oolitic sandstones and wackestones (LF1) and oolitic packstones-grainstones (LF2) in a Frías-Moscardón roadcut. Medium-scale cross-bedded oolitic grainstones with reactivation surfaces (dashed black line) and tabular beds on top, with local burrowing. **(B)** Meter-scale cycles of alternating marls and oolitic wackestones in LF1 (black arrows) and lateral transition to LF2 in Moscadón. **(C)** Burrowed packstone (detail of LF2 in A. **(D)** Wedge of clinobedded oolitic grainstones (LF3), interbedded with trough cross-bedded grainstones (LF4-1) and structureless and bioturbated (LF5) oolitic grainstones in Frías. **(E)** Clinobedded oolitic grainstones (LF3) overlaying oolitic packstones-grainstones (LF2) in Moscardón.

Fig. 3. Lithofacies LF1, LF2 and LF3. **(A)** Oolitic wackestone (LF1) polished slab with ferruginized ooids; matrix consists of lime mud and fine sand-sized quartz grains. **(B)** Polished slab of oolitic packstones-grainstones (LF2). **(C)** Outcrop view of clinobedded oolitic grainstones (LF3) with parallel lamination, marked by different grain sizes (arrows). **(D)** Polished slab: well- to moderately sorted ooids in clinobedded oolitic grainstones (LF3). **(E)** Photomicrograph of small ooids with thinly laminated fine-radial cortices, and larger ooids with alternating thin fine-radial and micritic laminae in LF3; oncoids (on) and aggregated ooids (ag) are also present. (**F)** Polished slab of the lowermost clinobeds (LF3) in Moscardón with oolitic intraclasts, compound ooids (co) and aggregated ooids (ag).

Fig. 4. Lithofacies LF4 (trough and planar cross-bedded oolitic grainstones) and LF5 (structureless to poorly laminated oolitic grainstones). **(A)** Decimeter-thick sets of trough cross-bedded grainstones (LF4-1). **(B)** Isolated sets of planar cross-bedded grainstones (LF4-2). **(C, D)** Polished slabs of LF4 grainstones; they are usually well sorted, and ooids have variable sizes and frequent quartz grains at their nuclei. **(E)** LF5 oolitic grainstones are poorly parallel- to undulate laminated, structureless or bioturbated; they occur in decimeter- to meter-thick beds. **(F)** Polished slab of well-sorted LF5 grainstone with compound ooids (co).

Fig. 5. (A, B) Mapped photomosaics and **(C)** sketches of the architecture of facies LF6, LF7 and LF8 in Frías (see location in Figs. 1 and 9). LF6 occur in continuous beds (see level 1 in C) or in lenticular and channel-like beds (see level 2 in C). **(D)** Metazoan-dominated mounds (LF7-1) include abundant corals and stromatoporoids, usually in growth position (see levels 1, 2 and 3 in C) and result from the amalgamation of small stratiform biostromes (see thin black lines in A and B). **(E)** Microbial crust-dominated mounds (LF7-2) dominate in the upper part of the outcrop (see levels 4 and 5 in C); the microbial crusts, with bush-like dendrolite fabric (see mc), surround the metazoan skeletons (e.g., st: stromatoporoids). Sandy intraclastic-oolitic packstones-grainstones (LF8) occur in inter-mound space and include abundant quartzite pebbles in level 5.

Fig. 6. Lithofacies LF6 (oolitic-skeletal grainstones with stromatoporoids), LF7 (mounds) and LF8 (sandy intraclastic-oolitic packstones-grainstones). **(A)** LF6: Stromatoporoids (st) in growth position surrounded by oolitic-skeletal grainstone matrix (mx). **(B)** Photomicrograph of the oolitic-skeletal grainstone matrix in LF6; it includes bioclasts (e.g., e: echinoderms), poorly sorted ooids with thinly laminated fine-radial and micritic cortices, compound ooids (co), and intraclasts made of oolitic facies (oi) and microbial crusts (mi). Bioturbation (b) is frequent. **(C)** Photomicrograph of a metazoan-dominated mound (LF7-1); it includes corals (c), discontinuous microbial crusts (mc) with micro-encrusters (k: *Koskinobullina*), and internal cavities filled by mud-supported sediment with fine sand-sized quartz grains, ooids (o) and bioclasts (l: lituolids). **(D)** Photomicrograph from a (LF7-2) mound dominated by microbial crust (mc), with micro-peloidal microfabric, abundant *Tubiphytes-Crescentiella* (tb) and small internal cavities (cv). **(E)** Photomicrograph of sandy intraclastic-oolitic packstones-grainstones (LF8), from the side of a metazoan-dominated mound. **(F)** Photomicrograph from a microbial crust-dominated mound. Both E and F are characterized by abundant fine sand-sized quartz grains, poorly rounded intraclasts of microbial crusts (mi), bioclasts (st: stromatoporoids, e: echinoderms) and variable proportion of reworked ooids (o).

Fig. 7. (A) Field image and synthetic log of the Pozuel Formation in the gully northwest of Frías. From base to top: vertically stacked beds with LF4, LF5 and LF6 oolitic facies, overlain by an intermediate level including mounds and related facies (LF6 to LF8), and mudstones, sandstones and conglomerates (LF9). **(B, C, D)** Siliciclastic facies on top of the oolitic succession consists of (B) sandstones with high-angle planar cross-bedding (LF9-1) that basinward pass into (C) through cross-bedded sandstones (LF9-2) overlain by low-angle cross-bedded sandstones (LF9-3) and bioturbated mudstones and planar cross-bedded sandstones with opposite inclination (LF9-4).

Fig. 8. Facies architecture of the Pozuel Formation near Moscardón (see Fig. 1A). **(A)** Facies architecture of accretional units M6 and M7 as seen in the cliff westward of the village. **(B)** In the entire outcrop, up to nine accretional units (M1 to M9) are stacked in an overall aggradational-progradational configuration. **(C)** Reconstruction of the stacked accretional units in B. Bed tilting has been restored by 5º clockwise rotation. Accretional units M1 to M9 can either be basic sequences or parasequences.

Fig. 9. (A) Facies architecture of the Pozuel Formation near Frías (Fig. 1A). **(B)** The lower accretional unit F1 is poorly exposed and is dominated by siliciclastic facies. Accretional units F1 and F2 are dominated by grain-supported oolitic facies. **(C)** The upper accretional units F4 and F5 contain various types of metazoan- and microbial crust-dominated mounds (see Fig. 5 for details). Accretional units F1 to F5 can either be basic sequences or parasequences

Fig. 10. Vertical facies succession of the Pozuel Formation and stacking of accretional units C1 to C8 in the Calomarde roadcut (see Fig. 1A). Accretional units C1 to C8 can either be basic sequences or parasequences

Fig. 11. Depositional model for the oolitic Pozuel Formation. Oolites were produced on the high-energy outer shelf (LF4-1) from where they were shed off downslope, building out a low-angle (5–10º) clinobedded lithosome (LF3). Downslope, the clinobedded lithosome interfingers and overlies the packstone toesets-bottomsets (LF2) and basinal marls (LF1). Updip, the foresets pass into sub-horizontal beds (topsets) with several lithofacies: through cross-bedded oolitic grainstones (LF4-1) produced by bedform migration in the outer part of

the shelf, and then into structureless grainstone (LF5) and then into mound-dominated lithofacies (LF7 and LF8) and into littoral-related lithofacies: oncolitic/peloidal packstones (LF10) and mudstone, sandstones and conglomerates (LF9). Planar cross-bedded grainstones (LF4-2) interbedded in structureless grainstones LF5 is thought to represent subaqueous dunes migrating on a stabilized and churned oolitic seafloor.

Fig. 12. Speculative correlation of the three studied localities, with hypothetic facies architecture.

Fig. 13. Line drawings of a high-resolution seismic line from the Holocene Faro Infralittoral Prograding Wedge, SW Spain (from Lobo et al., 2005). The internal architecture of the ILPW consists of a complex stack of shingled clinobed packages with oblique-tangential to sigmoidal reflection patterns. These packages are bounded, updip by erosion surfaces and downdip by the correlative conformities. These packages are thought to reflect changes in the magnitude and/or direction of storm events and associated downwelling storm currents, and/or climatically induced changes of sediment supply. Low-amplitude sea-level fluctuations may be the drivers of the stacking patters of these packages.

Fig. 14. Relationships between bedding patterns, facies architecture and bounding surfaces with the changes in the base level (adapted from Pomar and Tropeano, 2001). **(A)** During stillstand of sea level, wedge-shaped units prograded; subhorizontal beds (topsets) overlie and pass, basinward, into clinobedded slope (foresets) that basinward, in turn, interfinger and downlap onto fine-grained offshore deposits (bottomsets) (wbl: wave base level). **(B)** A subsequent fall of sea level, and concomitant lowering of base level, produces erosion of the topsets and increase sediment supply to the slope. The increase in sediment supply results in an increased dip angle of the clinobeds that downlap onto the downlapping clinobeds creating the “internal downlap surface” (dls). Sigmoidal to oblique-tangential bedding pattern characterize these units; note the resulting wedge is composed by three architectural elements: truncated still-stand prograding wedge (non-regressive progradation), regressive progradational wedge, and regressive prograding beach/beach ridges. **(C)** Architectural relationships and bounding surfaces between the beach, beach ridges and truncated clinobedded lithosome.

Fig. 15. **(A)** Relationships between the coeval coastal plain and Infralittoral Prograding Wedge prograding during the Holocene stillstand of sea level (modified from Fernández-Salas et al., 2009). In coasts with high sediment supply, longshore currents produce significant littoral drift and accretion of a bipartite succession of ILPWs and coastal-plain deposits (beach and beach-ridges), being both physically and genetically connected (from Fernández-Salas et al., 2009). **(B)** Bipartite shallowing-upward sandy succession formed under falling sea level. Two prograding units separated by a wave-erosion surface occur: the beach and the ILPW, being the lower boundary of the ILPW a downlap surface (from Fraser et al., 2005).

Fig. 16. Cliffy outcrops of the clinobedded grainstone wedges near the Capodarso bridge, Sicily. **(A)** A lower wedge (about 22 m thick) with oblique-tangential clinobeds (foresets) and a sub-horizontal package on top (topsets), overlain by a second prograding wedge. **(B)** Topsets and foresets in the lower wedge are defined by well-developed sigmoidal bedding; backsets (upslope-dipping cross-bedded bodies) occur within the foresets. **(C)** Detail of clinobeds downlapping onto the finer grained basinal deposits.

Fig. 17. (A) Vertical facies succession in Pleistocene prograding wedges with clinoform geometry, in the Crotone basin, south Italy. The synthetic log is based on a number of partial sections (from Massari et al., 1999). **(B**) Paleocurrents in the topset beds are more variable than in the foreset beds, where dip of cross-bedded intrasets approximates the clinoform dip.

Fig. 18. Simplified cross section of the oolitic prograding lithosome in the Aalenian/Bajocian Amellago ramp, in the Central High Atlas, Morocco. The section was made from correlation of logs in the high-frequency cycle 2a (modified from Pierre, 2006). The evolution of the depositional model along timelines is deduced from these correlations.

Fig. 19. The Smackover Formation in north-central U.S. Gulf Coast. **(A)** Conceptual sequence stratigraphic model (modified from Heydari and Baria, 2005). **(B)** Log interpretation of the Brammer no. 1 North American Timber well, based on the physical attributes (modified from Handford and Baria, 2007). **(C)** Clinoforms within the middle to upper Smackover "B" Formation showing downlap and toplap surfaces; progradation was to the southwest. Reproduced with permission of Jura-Search Inc. (Jackson, MS, US).

Fig. 20. Distribution of the Hanifa shallow-shelf facies in the Khurais Complex, prograding (black arrows) on the margins of the Arabian basin. Paleogeography based on Ziegler (2001).

Fig. 21. Lithologic logs of the Hanifa Formation in Khurais Complex, from cores in the Mazlij (MZLJ) and the Khurais (KHRS) oil fields. Grainstones of the Hawtah Member mostly composed by well-sorted peloids occur on top of a muddy succession, with either transitional or sharp contact. In the peloidal grainstones, a homogeneous lower interval can be differentiated from a heterogeneous upper interval by differential bedding and/or the presence of large skeletal fragments. Coral and stromatoporoid bioherms commonly overlie the grainstone unit, and those, in turn are overlain by the lime-muds and stromatoporoid-microbial bioherms of the Ulayyah Member.

Fig. 22. Conceptual model for the *Infralittoral prograding wedges* (ILPW). Grain-dominated carbonate sediments, are mostly produced within above wave base. Waves and associated currents (downwelling, rip and longshore) stir the sediments and move them obliquely (downdip and alongshore). Sediments swept seaward from the friction-dominated zone during events of intense wave action, will avalanche on the slope, below the wave base, and episodically move down as gravity flows. This cause the grain-dominated slope deposits to prograde on basinal muds. The types of carbonate grains produced in the shallow platform vary through time, depending on the changes in the carbonate factories induced by biological evolution and by changes in paleo-oceanographic conditions.

LF1	**Marls and intercalated oolitic sandstones and wackestones**	Marls with abundant mica and plant remains, and scarce bioclasts (bivalves, brachiopods, gastropods and foraminifera). Abundant bioturbation.
LF2	**Oolitic packstones-grainstones**	Oolitic packstones-grainstones in thin to medium beds interbedded with cm-thick marly beds. Locally with medium-scale cross-bedding. Minor components are sand-sized quartz grains, peloids and bioclasts. Brachiopods, echinoids and scallops are frequent.
LF3	**Clinobedded oolitic grainstones**	Oolitic grainstones with variable-sized ooids, well to moderately sorted, in medium to thick beds forming large-scale clinobeds dipping around 5º to 10º
LF4	**Trough- or planar cross-bedded oolitic grainstones**	**LF4-1:** Very-well- to well-sorted oolitic grainstones, in sets up to 50 cm thick with trough cross-bedding **LF4-2:** Up to 2-m thick very well- or well-sorted oolitic grainstones with planar cross-bedding at dune-scale.
LF5	**Structureless to poorly laminated oolitic grainstones**	Well-sorted oolitic grainstones arranged in 0.3- to 1-m thick tabular beds, with poorly developed parallel to undulate lamination.
LF6	**Oolitic-skeletal grainstones with stromatoporoids**	Oolitic-skeletal grainstones with abundant stromatoporoids in thin tabular beds or lenticular to channel-like bodies. Stromatoporoids are in situ in the tabular beds or as rubble at the base of lensoidal bodies.
LF7	**Mounds**	**LF7-1**: Decimeter- to meter-scale mounds dominated by corals, stromatoporoids and chaetetids. **LF7-2**: Decimeter- to meter-scale mounds dominated by microbial crusts with micro-peloidal fabric to dendrolitic. Corals and stromatoporoids are also present.
LF8	**Sandy intraclastic-oolitic packstones-grainstones**	Decimeter-thick fine-grained sandy intraclastic-oolitic beds with thin marly intercalations. Abundant fine sand-sized quartz grains, poorly rounded intraclasts of microbial crusts, bioclasts and variable proportion of ooids. This facies occur as inter-mounds sediments.
LF9	**Mudstones, sandstones and conglomerates**	With diverse sedimentary structures (low-angle and high-angle planar cross-bedding, trough cross-bedding, bioturbation) and variable proportion of ooids, quartzite and carbonate pebbles.
LF10	**Oncolitic/peloidal packstones**	Thin to medium tabular beds of packstones with oncoids and peloids, and minor proportion of bioclasts, intraclasts and ooids.

Table 1. Lithofacies

	Trincardi and	**Tesson et al.,**	**Hernandez-Molina et al.**	**Chiocci and**	**Chiocci et**	**Chiocci et**	**Chiocci et**

	Field (1991)	(1993)	(1995, 1998)	Orlando (1996)	al. (2004)	al. (2004)	al. (2004)
LOCATION	Tyrrhenian Sea (Italy)	Rhône continental shelf (France)	Cabo de Gata/Alboran Sea (Spain)	Tyrrhenian Sea (Italy)	Capraia	Elba W	Pontine Islands SE
AGE	Late Pleistocene	Late Pleistocene-Holocene	Holocene	Holocene and Late Pleistocene	Late Pleistocene	Late Pleistocene	Late Pleistocene
LATERAL EXTENT of tabular bodies	9–38 km	over the entire shelf (35–70 km)	laterally extensive	as long as shelf conditions persist	15 km	25 km	23 km
WIDTH (progradation)	1–10 km	up to 40 km (2)	300 m	up to 1 km	0.5–1 km	0.5–0.75	0.7–2 km
THICKNESS of tabular sets	10–12 m 30–60 m	up to 30 m	up to 30 m	20–30 m	0.5–1 m	20 m	34 m
CLINOBEDS DIP (angle of repose)	1.5°	1.5°		5° - 9° if >10° is transparent	15°	15°	> 10°
GRAIN SIZE		fine-grained sand and silt	fine-grained sand and silt	sand and silt	Coarse to medim sand		
SEDIMENT TYPE		siliciclastics	siliciclastics	intrabasinal sediments mainly bioclastic	bioclastic coarse to medium-coarse sand		
UPPER BOUNDARY	toplap (erosion surface of ravinement)	toplap surface	toplap surface	toplap surface			
LOWER BOUNDARY	downlap surface	downlap surface	downlap surface	downlap surface			
INTERPRETATION	beach-shoreface progradation during sea-level fall and lowstand	parasequences or high-frequency sequences wave-dominated coastal progradation by longshore drift	progradation of the infralittoral wedge during stillstand (Holocene highstand) of sea level	deposition bellow storm-wave base during stillstand of sea level			
NAME	downlapping regressive shelf deposits	shelf prograding sediment wedges	infralittoral prism	submarine terrace deposits	depositional terraces	depositional terraces	depositional terraces
EUSTATIC CONTEXT	related to the late glacial lowstand of sea level and transgression	Late Pleistocene high-amplitude sea-level fluctuations	Holocene highstand	Holocene highstand Mid-Late Pleistocene glacioeustasy with frequent stillstands			

Table 2: Characteristics of Holocene and Upper Pleistocene infralittoral prisms occurring in continental shelves of the Western Mediterranean

	Age	Composition	Width (dip)	Elongation	Thickness	Dip of x-beds	Shingled units	Top + clino + bottom	Downlap & interfingering basinal muds
Capodarso, Sicily	Pliocene	Skeletal	2 km	10's km	< 27 m	Few°-19°	**X**	**X**	**X**
Crotone, S. Italy	Pleistocene	Mixed	5 km	Confined basin	< 45 m	10°-16°	**X**	**X**	**X**
Amellago, Morocco	Aalenian/Bajocian	Oolitic-peloidal	> 5 km (10-15 km)	> 15 km	15-20 m	3°-4°	**X**	**X**	**X**
Las Pilas, N. Mexico	Albian	Oolitic	> 5 km	Outcrop limited	40-60 m	Master s. 8°-15° Foresets 1°-20°	**X**	**X**	**X**
Smackover, Louisiana, US	Oxfordian	Oolitic	> 19 km	6-16 km single unit Whole area of survey	50-70 m	4-7	**X**	**X**	**X**
Hanifa Saudi Arabia	Late Oxfordian early Kimmeridgian	Peloidal oolitic	150 km	> 100 km	12 to 15 m		**-**	X	X

Table 3. Characteristics of infralittoral prograding wedges hold by the examples here summarized

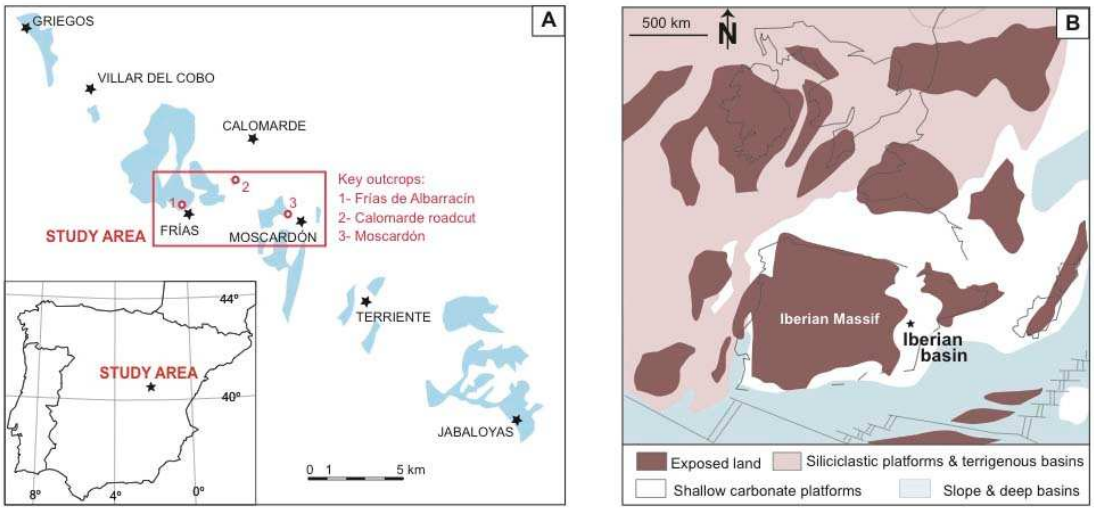
A
GRIEGOS
VILLAR DEL COBO
CALOMARDE
STUDY AREA
FRÍAS
MOSCARDÓN
Key outcrops:
1- Frías de Albarracín
2- Calomarde roadcut
3- Moscardón
TERRIENTE
JABALOYAS
STUDY AREA
44°
40°
8°
4°
0°
0 1 5 km
B
500 km
N
Iberian Massif
Iberian basin
Exposed land
Siliciclastic platforms & terrigenous basins
Shallow carbonate platforms
Slope & deep basins

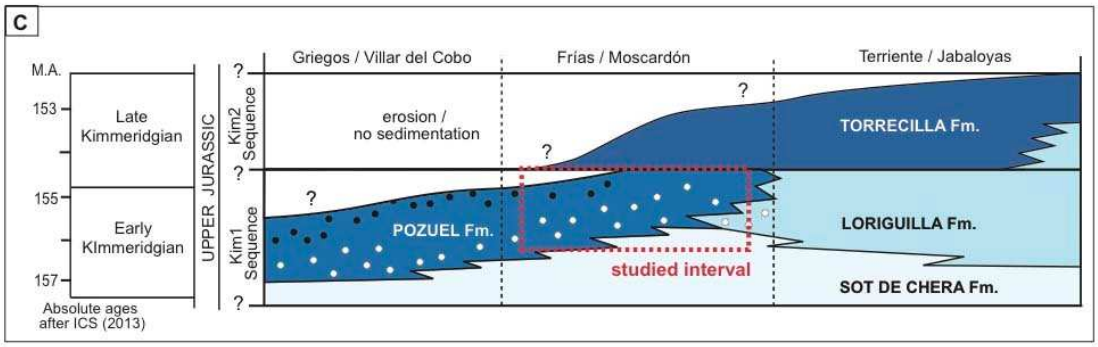
C
M.A.
153
155
157
Late Kimmeridgian
Early KImmeridgian
UPPER JURASSIC
Kim2 Sequence
Kim1 Sequence
Absolute ages after ICS (2013)
Griegos / Villar del Cobo
Frías / Moscardón
Terriente / Jabaloyas
erosion / no sedimentation
TORRECILLA Fm.
POZUEL Fm.
LORIGUILLA Fm.
studied interval
SOT DE CHERA Fm.

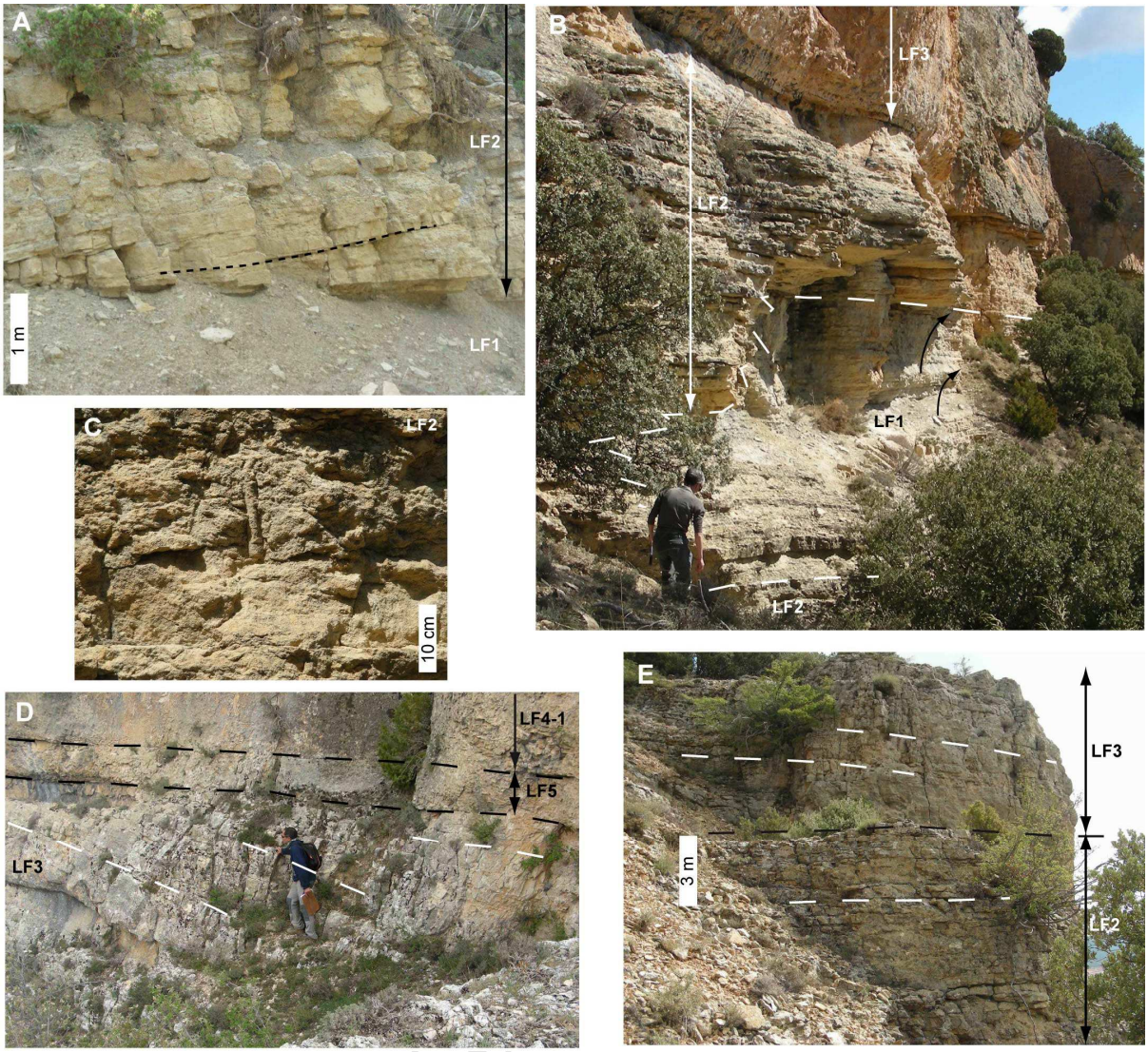
A
LF2
LF1
1 m
B
LF3
LF2
LF1
LF2
C
LF2
10 cm
D
LF4-1
LF5
LF3
E
LF3
3 m
LF2

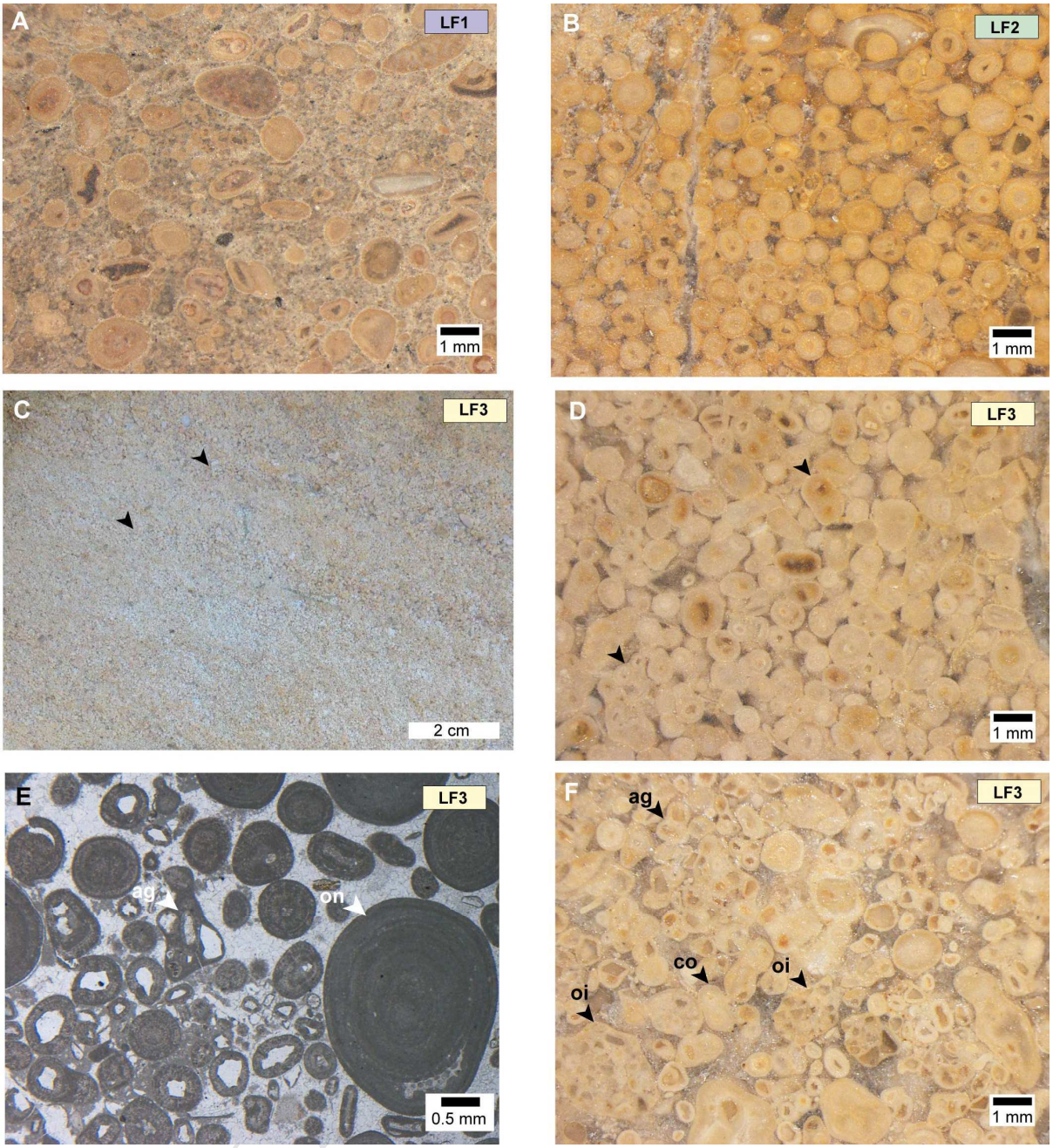
A
LF1
1 mm
B
LF2
1 mm
C
LF3
2 cm
D
LF3
1 mm
E
LF3
ag
on
0.5 mm
F
LF3
ag
co
oi
oi
1 mm

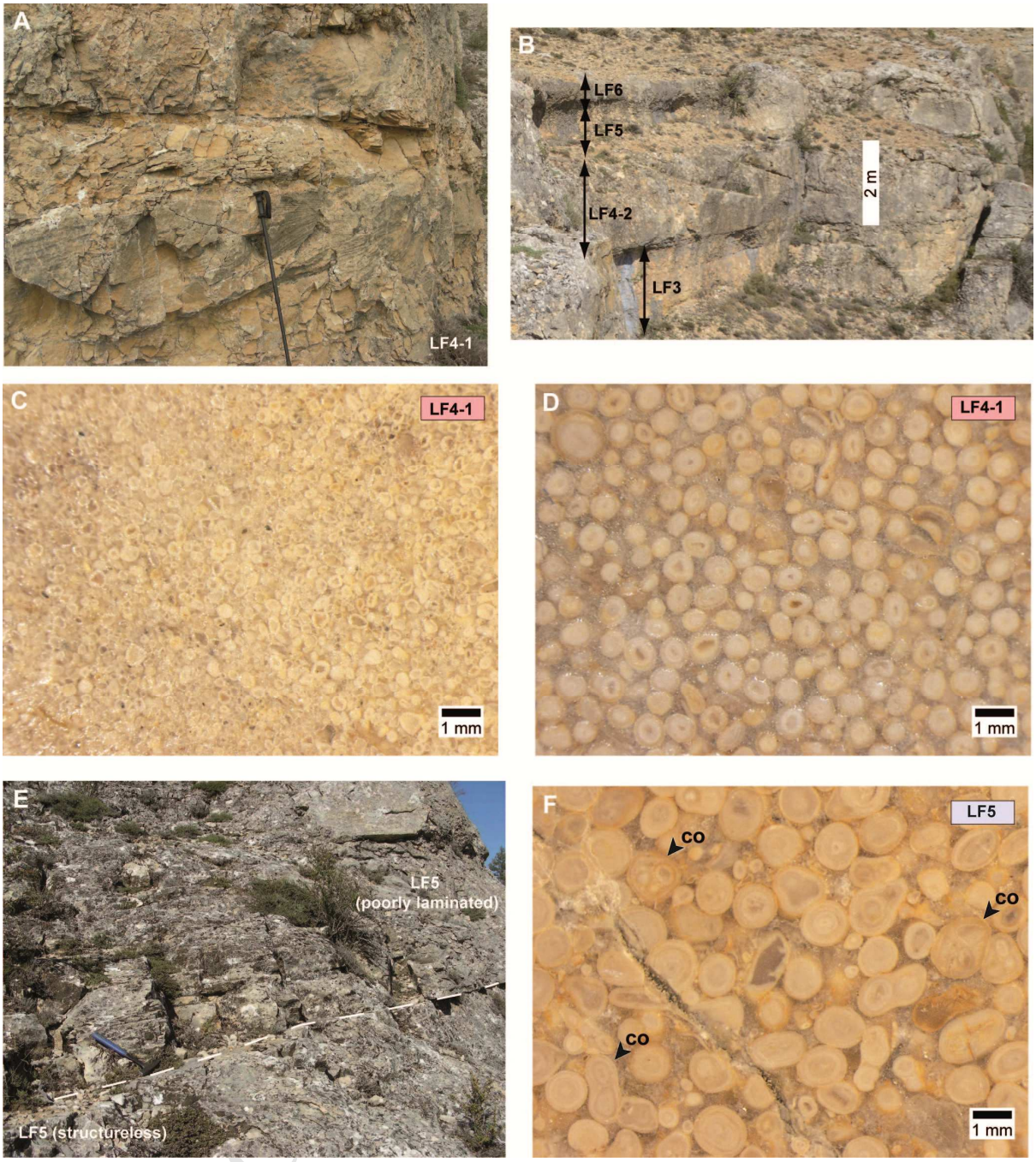
A
LF4-1
B
LF6
LF5
LF4-2
LF3
2 m
C
LF4-1
1 mm
D
LF4-1
1 mm
E
LF5
(poorly laminated)
LF5 (structureless)
F
LF5
CO
CO
CO
1 mm

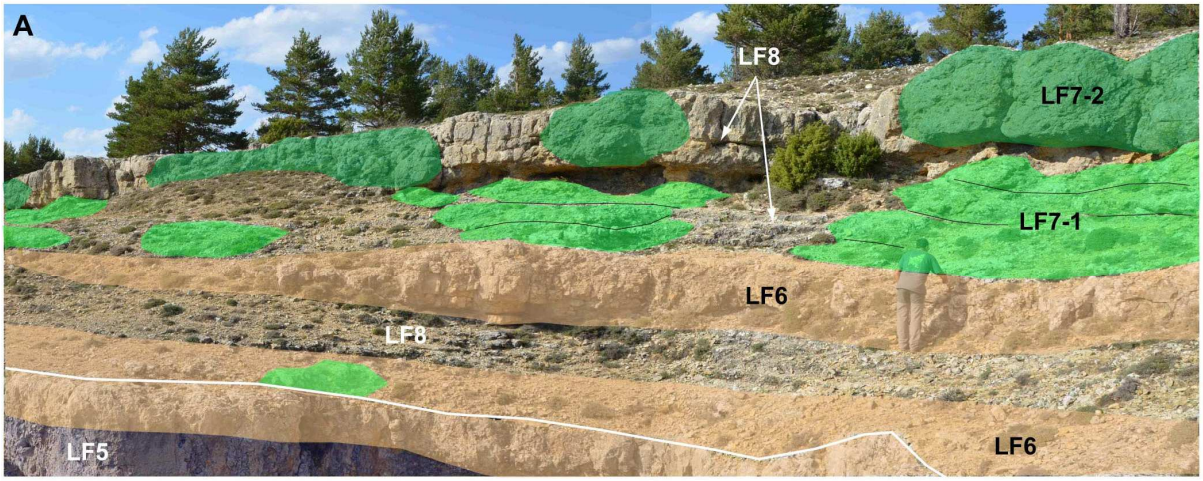
A
LF8
LF7-2
LF7-1
LF6
LF8
LF5
LF6


B
LF8
LF7-2
LF7-1
LF6
LF6
LF5

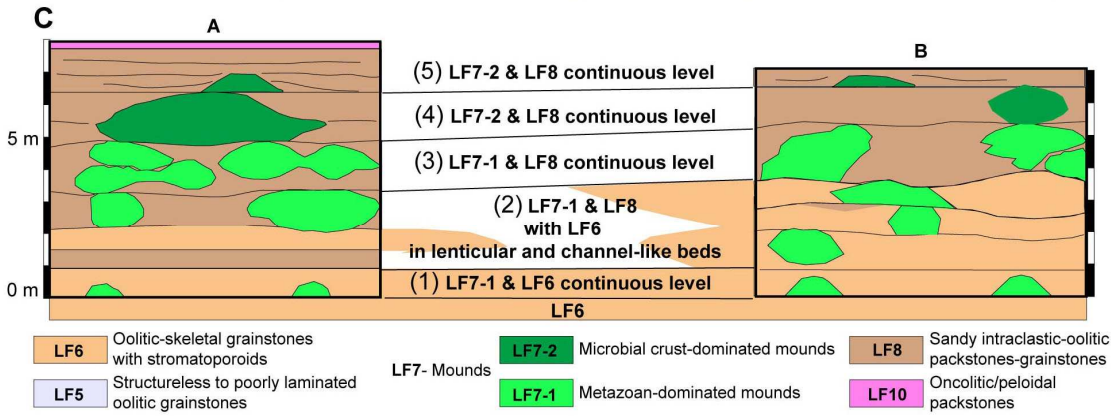
C
A
B
5 m
0 m
(5) LF7-2 & LF8 continuous level
(4) LF7-2 & LF8 continuous level
(3) LF7-1 & LF8 continuous level
(2) LF7-1 & LF8
with LF6
in lenticular and channel-like beds
(1) LF7-1 & LF6 continuous level
LF6
LF6 Oolitic-skeletal grainstones with stromatoporoids
LF5 Structureless to poorly laminated oolitic grainstones
LF7- Mounds
LF7-2 Microbial crust-dominated mounds
LF7-1 Metazoan-dominated mounds
LF8 Sandy intraclastic-oolitic packstones-grainstones
LF10 Oncolitic/peloidal packstones

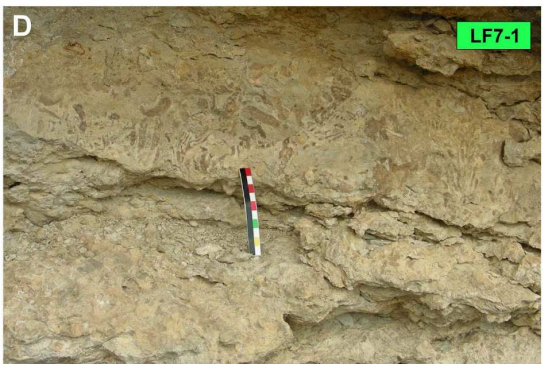
D
LF7-1


E
5 cm
LF7-2
st
mc

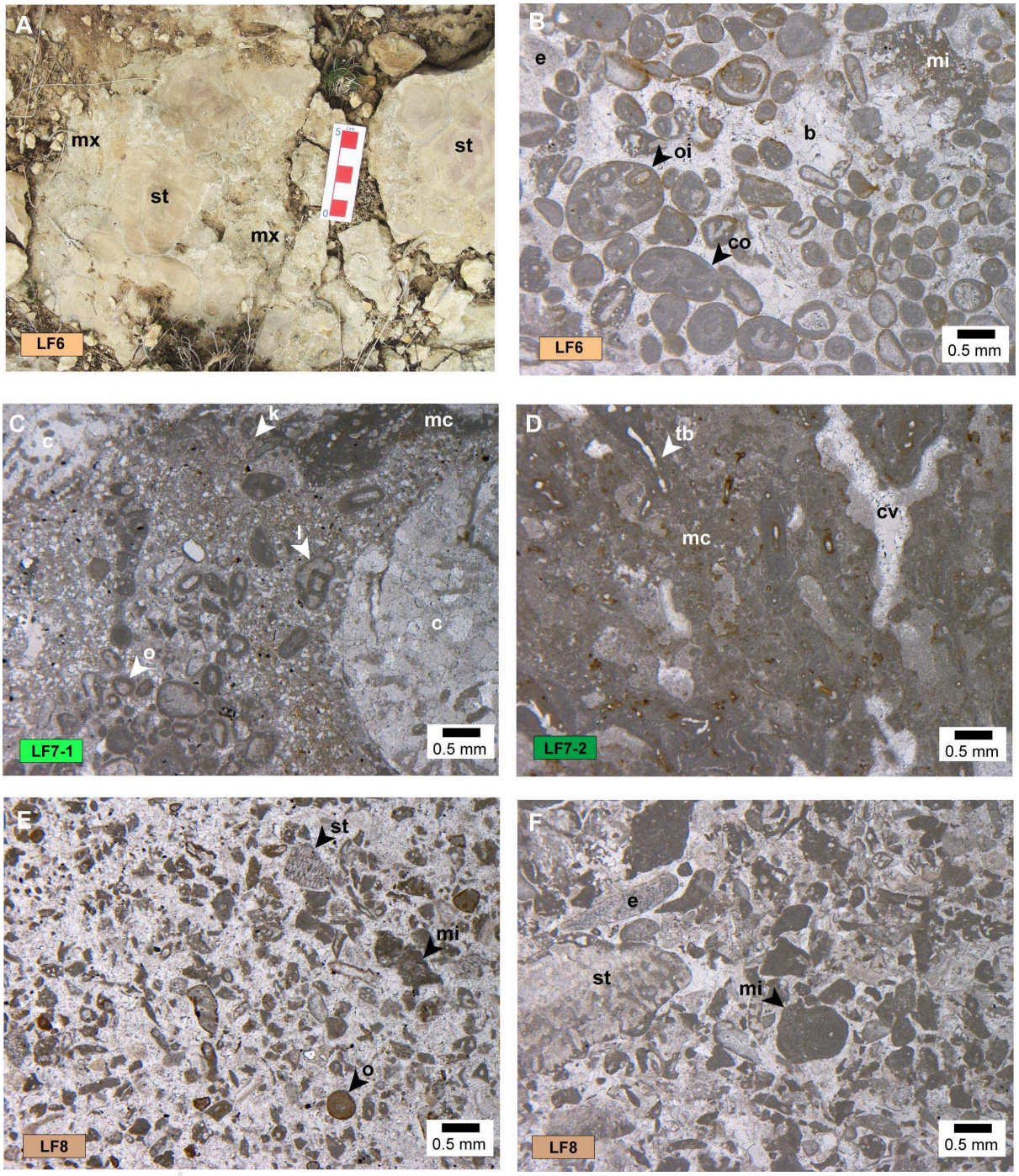
A
mx
st
st
mx
LF6
B
e
mi
b
oi
co
LF6
0.5 mm
C
c
k
mc
l
c
o
LF7-1
0.5 mm
D
tb
cv
mc
LF7-2
0.5 mm
E
st
mi
o
LF8
0.5 mm
F
e
st
mi
LF8
0.5 mm

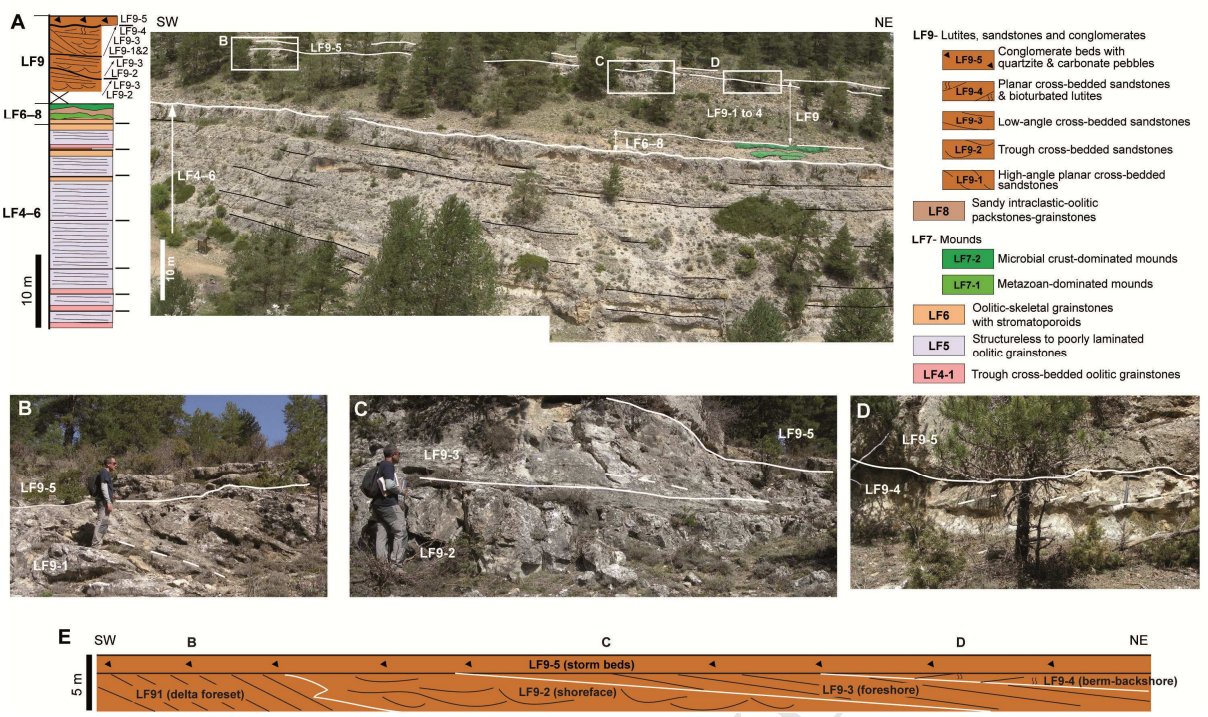

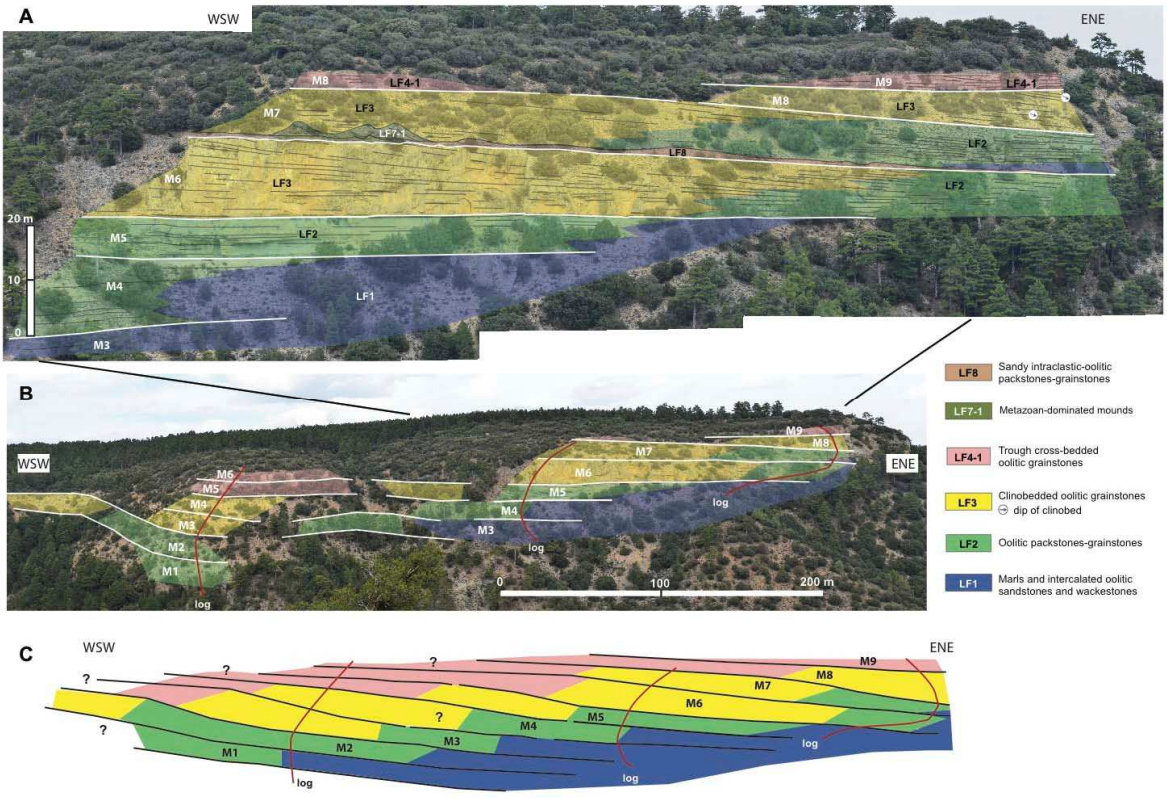

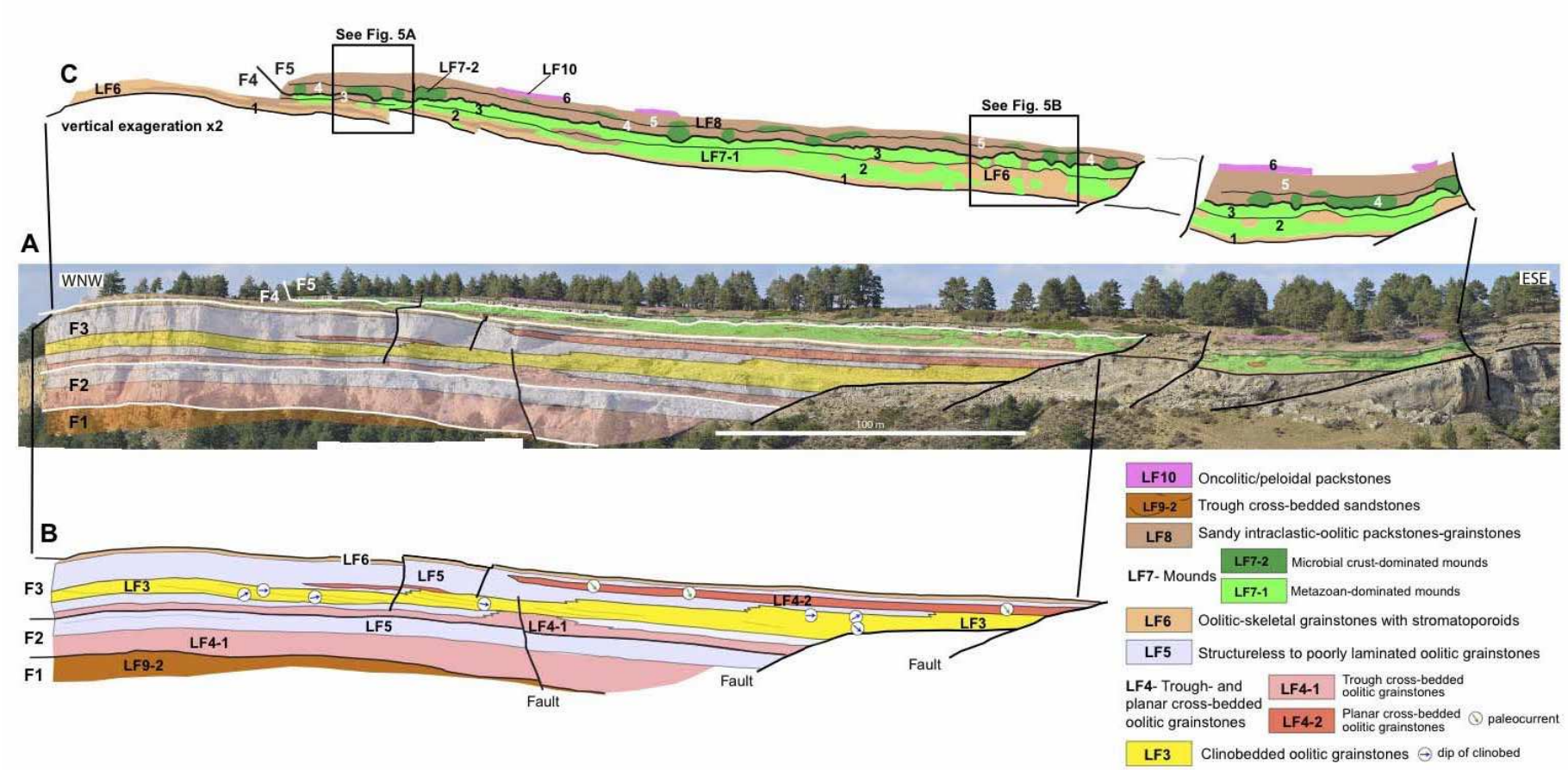

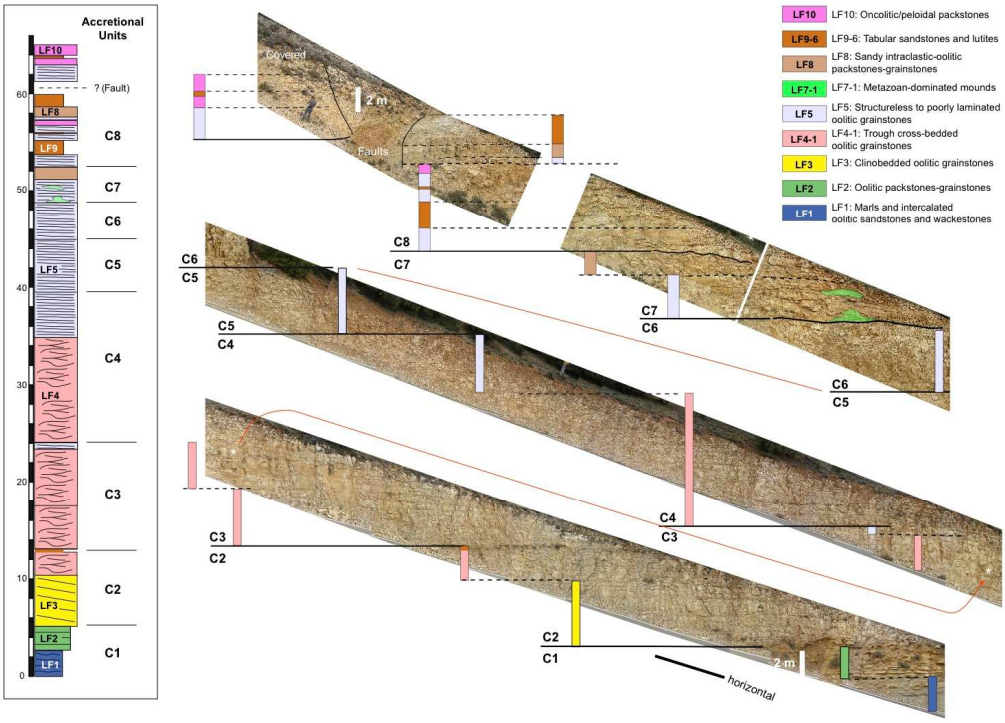

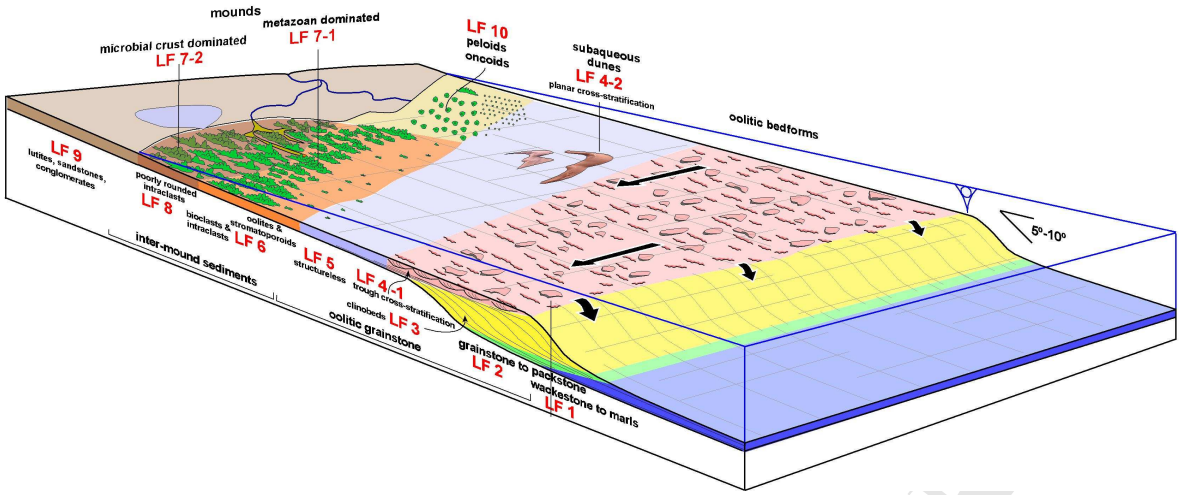

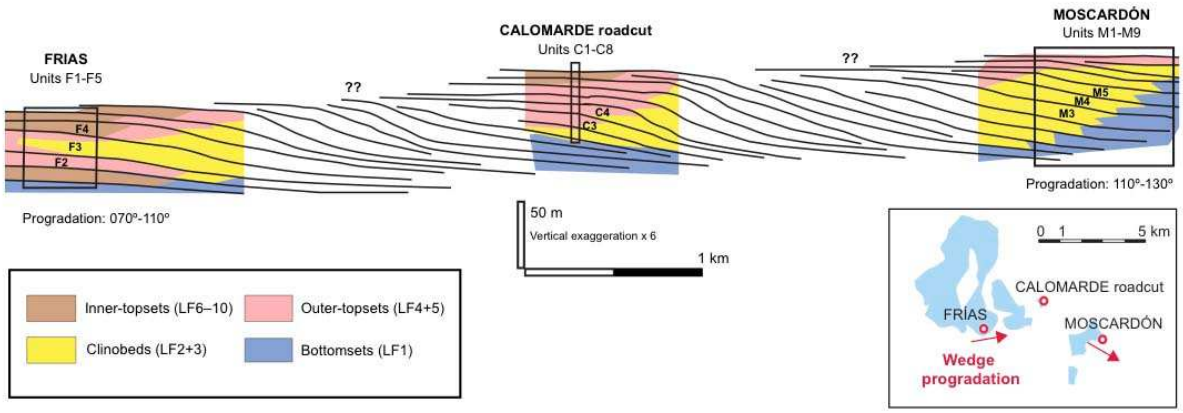

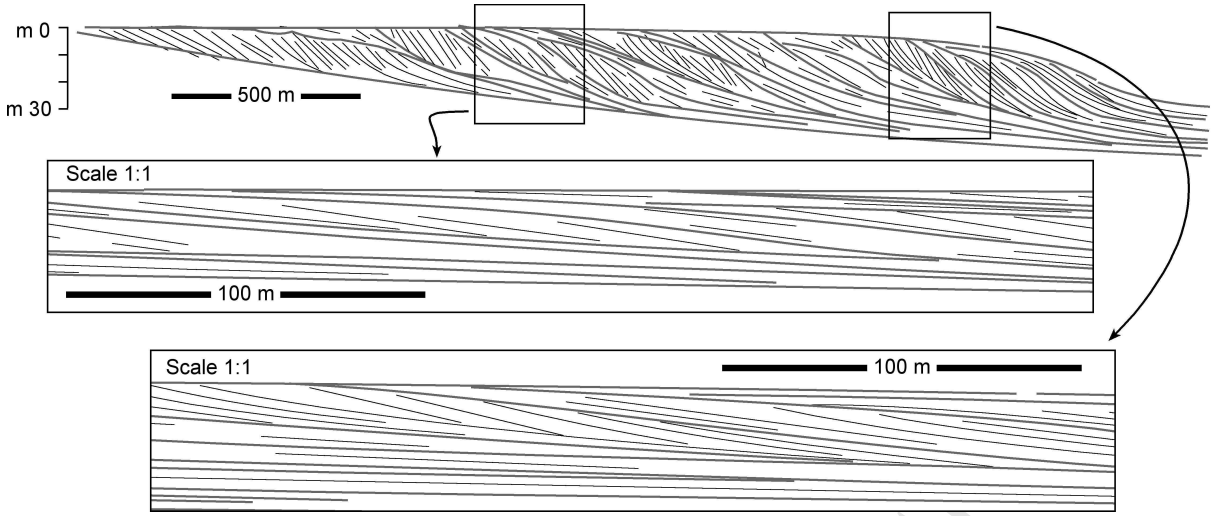

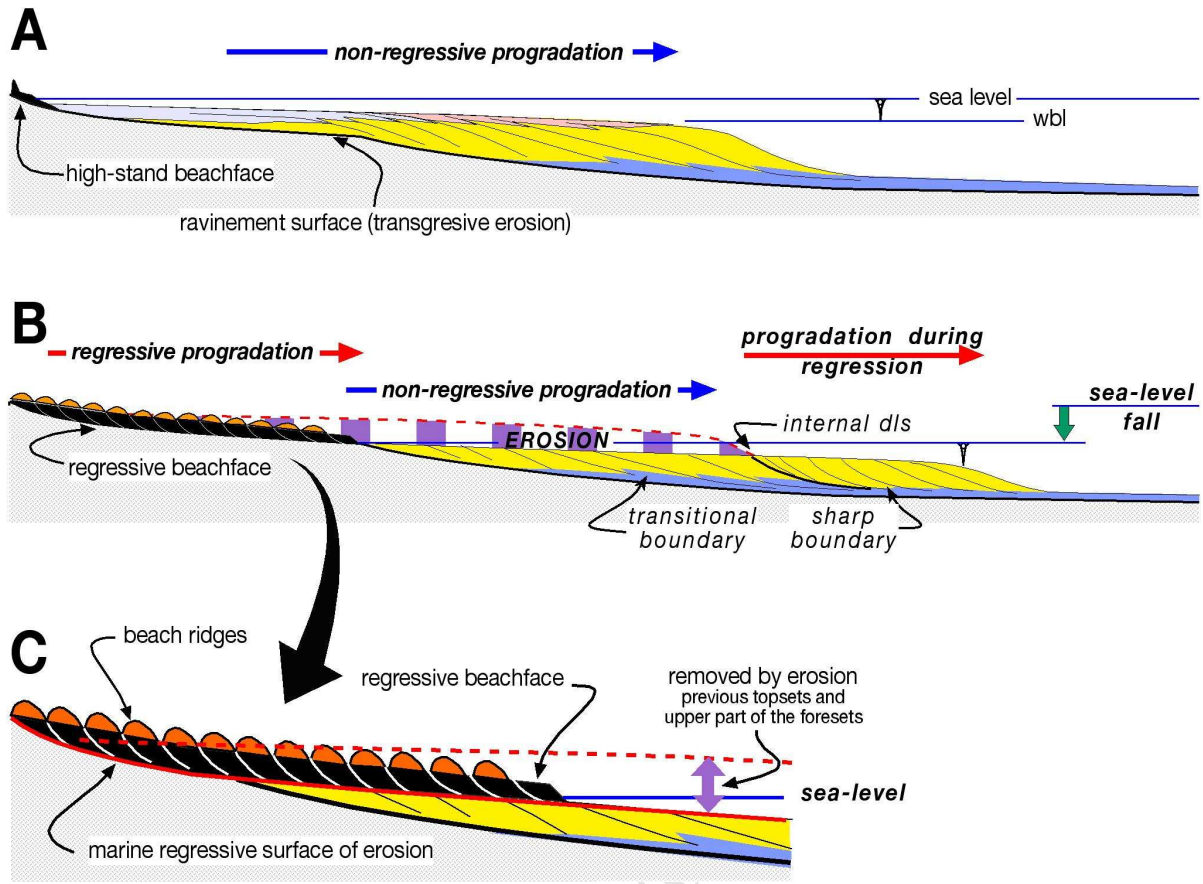

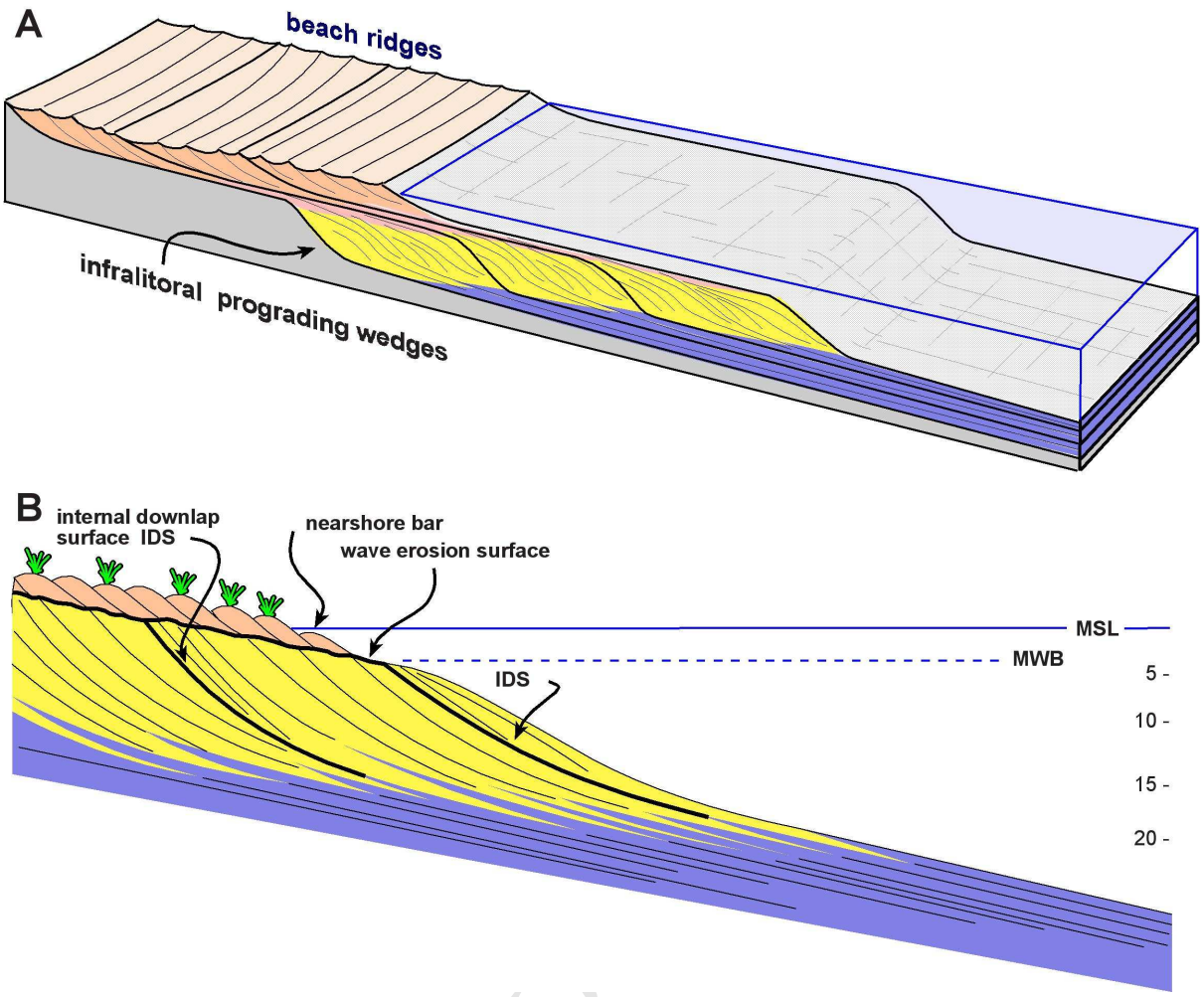
A
beach ridges
infralitoral prograding wedges
B
internal downlap surface IDS
nearshore bar
wave erosion surface
MSL
MWB
IDS
5 -
10 -
15 -
20 -

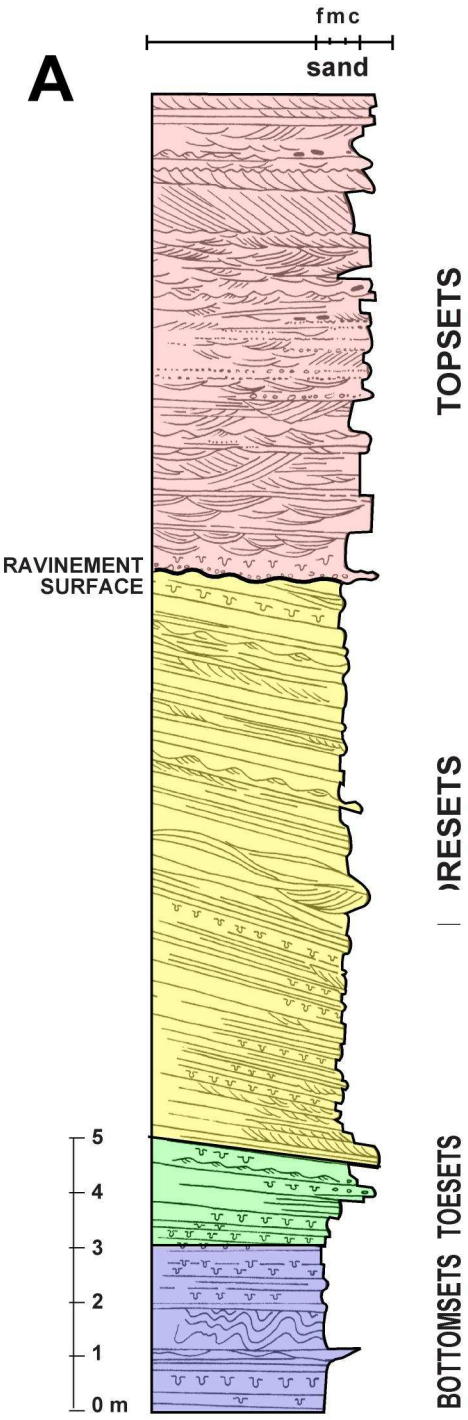

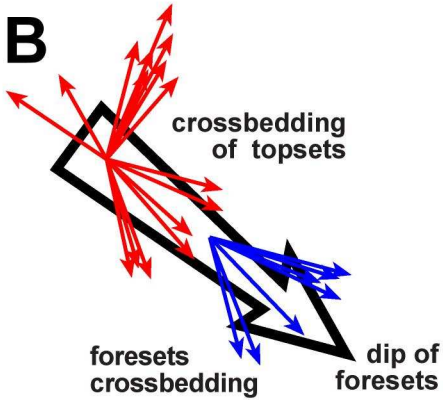

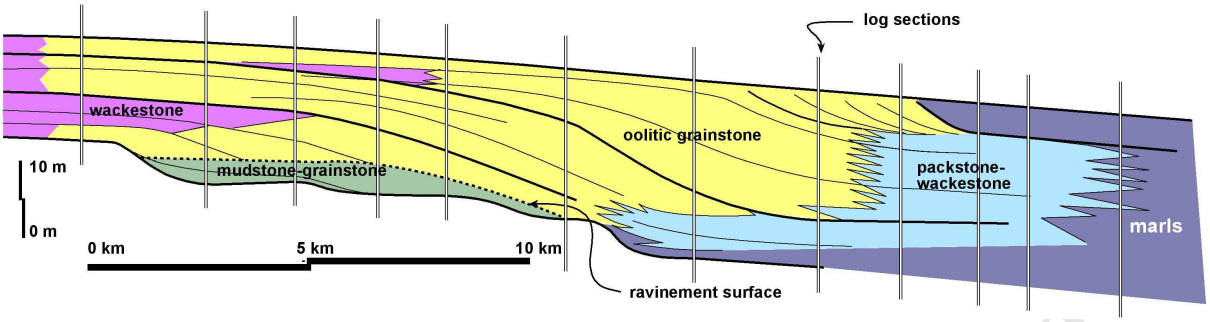

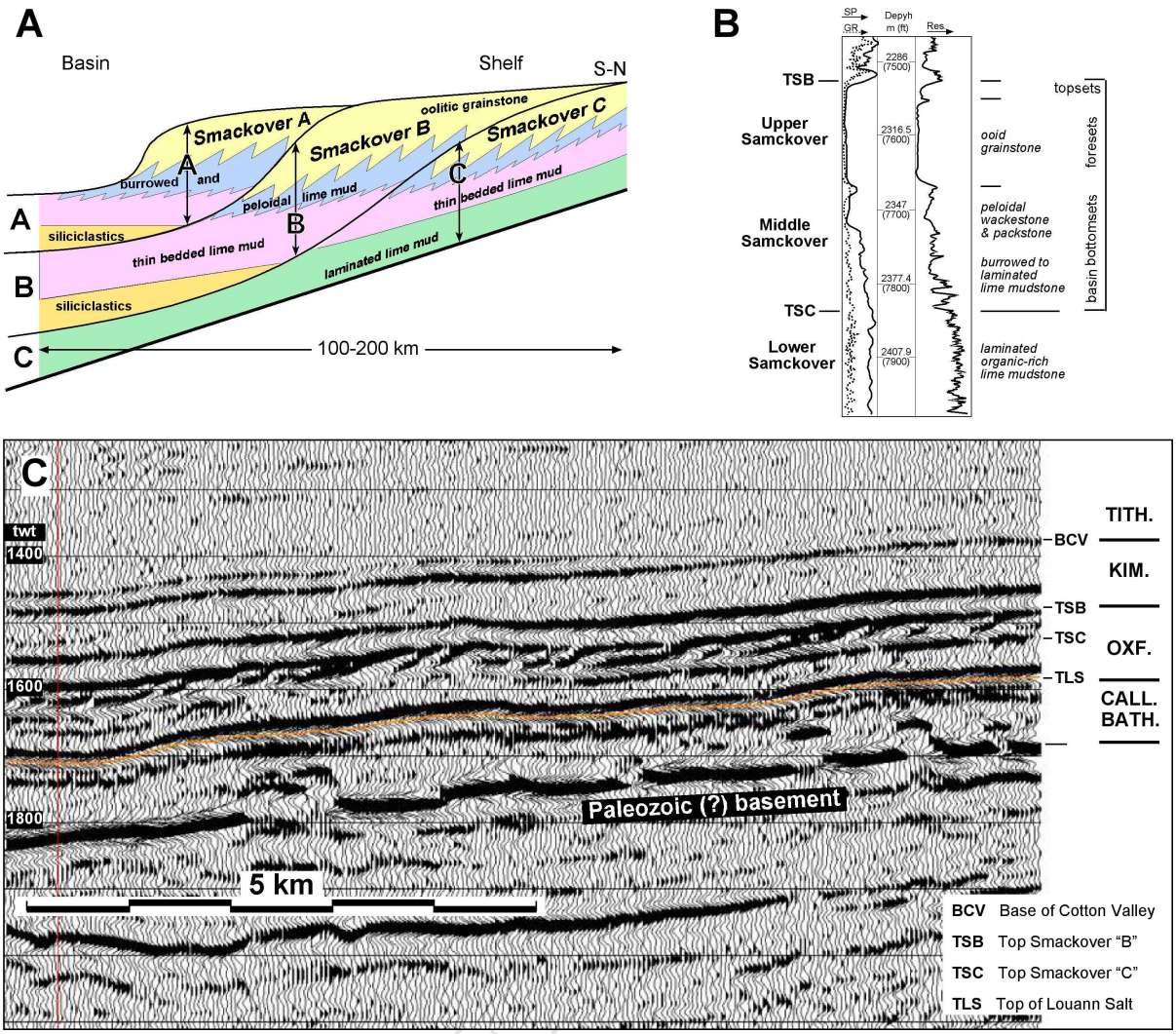

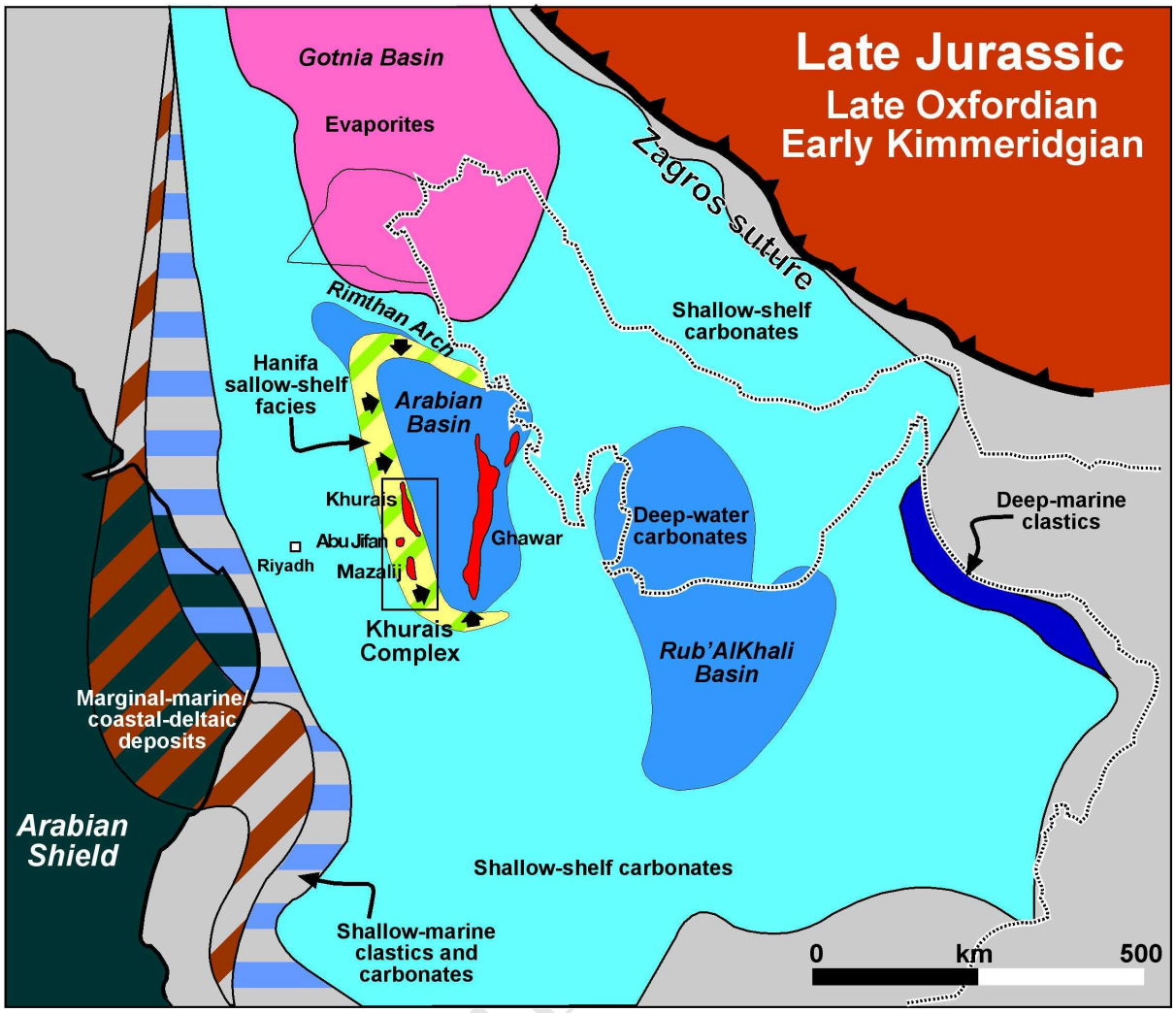

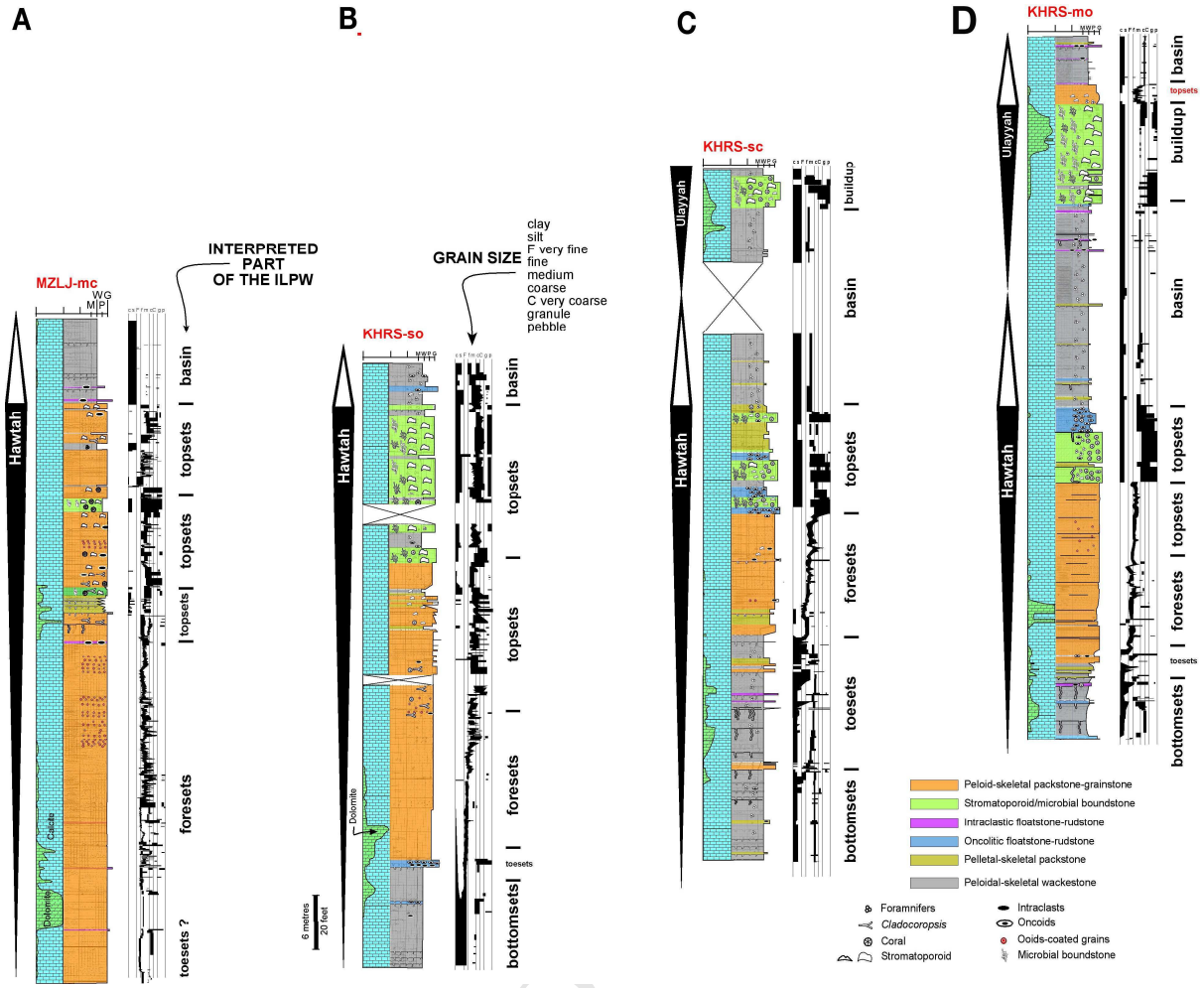

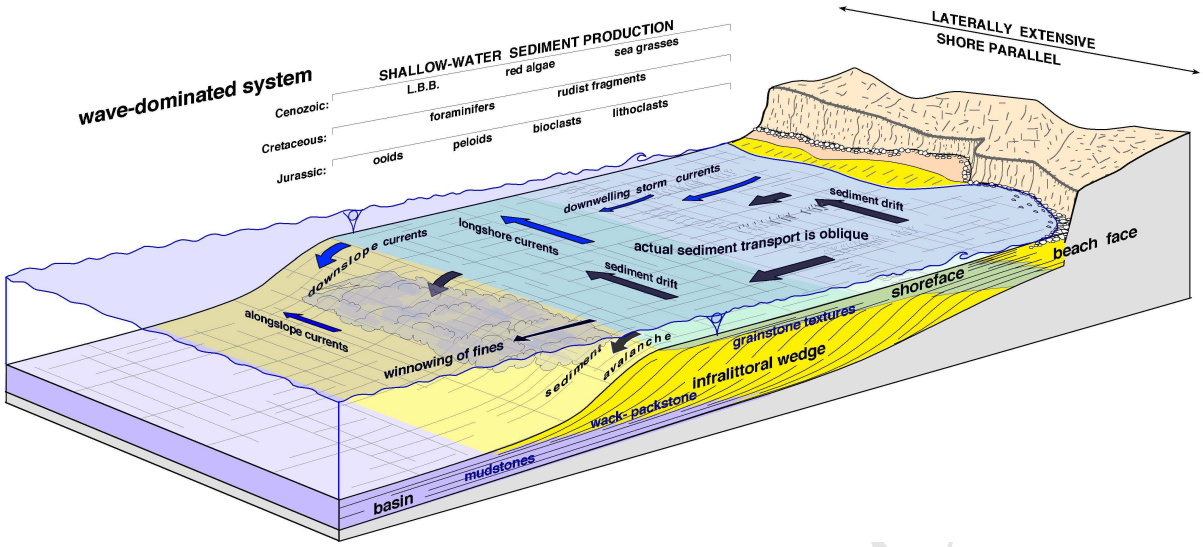

Highlights

Depositional model for a wave-dominated, strike-elongated, oolitic prograding wedge

The *infralittoral prograding wedge*, an alternative model for prograding sand-bodies

Factory along the wave-dominated platform, grains transported landward and seaward

Oolitic-grains cascaded below wave-base in the foresets form 5–10º dipping clinobeds

Field analog to stratigraphically equivalent subsurface reservoirs